# MODIFIED EUTECTIC ALLOYS

## FOR HIGH TEMPERATURE SERVICE

Second Year Interim Report

by

S. F. Ramseyer and J. F. Wallace

Department of Metallurgy

Case Institute of Technology

For Contract Period

May, 1965 to June, 1966

NASA Grant SC-NsG 639/36-~~033~~-033 $\overset{OO3}{}$

Prepared for

National Aeronautics and Space Administration

Lewis Research Center

Cleveland, Ohio

**Case Institute of Technology**

**10900 Euclid Avenue**

Cleveland, Ohio   44106

MODIFIED EUTECTIC ALLOYS

FOR HIGH TEMPERATURE SERVICE

Second Year Interim Report

by

S. F. Ramseyer and J. F. Wallace

Department of Metallurgy

Case Institute of Technology

For Contract Period

May, 1965 to June, 1966

NASA Grant SC-NsG 639/36-033-033

Prepared for

National Aeronautics and Space Administration

Lewis Research Center

Cleveland, Ohio


Case Institute of Technology

10900 Euclid Avenue

Cleveland, Ohio    44106

## INTRODUCTION

The control of as-cast structure is important for the development of optimum properties of an alloy. In recent years, much effort has been directed toward the development of techniques to control this structure for improvements in over-all properties and for specific applications. The methods for control of cast structure may be classified as: a) eutectic modification; b) grain refinement; c) directional solidification. These techniques are often used in conjunction with one another. This grouping was chosen primarily for convenience in discussing cast structure control.

A) Eutectic Modification:

In cast alloys, the term "modification" has most often been used when considering the aluminum-silicon eutectic system. It describes the microstructural change which occurs when these alloys are either rapidly cooled or slowly cooled after treatment with small amounts of sodium or other modifiers. The term has also been used to describe the formation of nodular rather than flake graphite in cast iron-carbon-silicon alloys of near eutectic composition which have been treated with small amounts of cerium or magnesium.

More recently, "modification" of eutectic alloys has been considered as a general phenomenon which occurs in

many systems, from low melting point eutectic alloys of lead-tin treated with copper[1] to the high temperature eutectic alloys studied under the present program. Although modification in most of the literature is applied only to systems where a third phase does not occur third phases often form in the present work and even completely replace one of the eutectic phases. Therefore, the definition of "modification" has been expanded and redefined as the change in microstructure after solidification of the eutectic brought about by the addition of one or more solute elements or by a change in cooling rate[2].

In developing the mechanisms of modification, both nucleation and growth conditions must be considered. The aluminum-silicon system has received the most attention, yet no general agreement on what controls modification in this alloy system has been obtained. Most investigations of the system tend to favor mechanisms which control one or the other condition rather than a combination. Yet a combination of mechanisms appears to be necessary to explain all the phenomena observed during solidification of aluminum-silicon alloys.

To understand the various proposed mechanisms more completely, the various phenomena observed during solidification of these alloys are reviewed.

1)   Rapid cooling produces a substantial refinement
     of the eutectic structure in the binary alloys.

2)   Small additions of sodium ($<$0.05%) and other
     elements (e.g. calcium, potassium, titanium)
     cause modification.(3)

3)   Alloys with phosphorus cannot be modified by
     rapid cooling, and increased amounts of sodium
     are required for modification of slowly cooled
     melts.(4)

4)   Alloys always undercool when modified, whether by
     rapid cooling or sodium addition, yet melt at the
     equilibrium melting temperature (5)

5)   The shape of the silicon particles seems to be
     more growth-temperature dependent, than alloy
     composition dependent.(6)

6)   The amount of sodium needed for modification is
     dependent on the silicon content of alloy.(7)

The influence of increased cooling rate on the
eutectic structure seems to be caused by the increased
supercooling in front of the solidifying interface and
decreased time for silicon to diffuse long distances.(3,8)

As suggested by Chadwick (3), the various theories of
modification of the aluminum-silicon eutectic alloys by
sodium addition can usually be placed in one of three

categories: (a) the formation of ternary eutectic between aluminum, silicon and sodium; (b) modification of the nucleation process by sodium poisoning; or (c) restricted growth of silicon caused by absorption of sodium. The work of Thall and Chalmers (5) seems to have disproved mechanism (a). The study of Kim and Heine (6) is representative of work in support of mechanism (b), while mechanism (c) is favored by Davies and West (4). Thall and Chalmers showed that a modified alloy always undercooled, while it melted at the equilibrium eutectic temperature; this refutes the suggestion (9) that a sodium addition caused a ternary eutectic to form.

The influence of phosphorus on the modification process seems to suggest that nuclei, possibly AlP (4) form and cause nucleation of the silicon phase at the equilibrium eutectic temperature. The initial sodium additions inactivate these nuclei, so additional sodium is needed to cause modification. This latter observation indicates a restricted nucleation mechanism for modification. This argument maintains that sodium affects the nucleating centers or substrates, either by destroying these or adsorbing onto these to form a "poison" layer which restricts their growth. The fact that silicon is growth-temperature dependent (6), rather than composition

dependent, is also presented as further evidence that
sodium affects nucleation rather than growth conditions.
Since increasing the silicon content increases the amount
of sodium needed for modification (7), it is suggested
that a relation exists between sodium and the amount of
silicon surface area on which sodium might be adsorbed.
Davies and West (4) favored growth modification on the
basis of observed changes in crystal habit of the silicon
in their sodium modified alloys; their interpretation of
the data of Plumb and Lewis (10) which showed that 3 to 4
times as much sodium was located around the silicon part-
icles as in the aluminum, also substantiates their argu-
ment. However, Chadwick indicates (3) that other in-
vestigations in the literature are in direct conflict
with Davies and West, particularly on the growth tempera-
ture dependence of silicon morphology.

Winegard and co-workers (11), working with ultra-
high purity Al-Si alloys, have found that the silicon is
not particulate, but interconnected within a eutectic
cell. Rapid cooling only decreases the cell size and in-
creases the number of arms or branches to the "silicon
tree" within each cell. This would explain Meussner's
observation that the silicon within a single eutectic
aluminum grain was aligned.(12)   Thus, despite the

relatively extensive investigation carried out on the aluminum-silicon system, no general agreement exists on why modification occurs.

The role of constitutional supercooling in determining morphology of eutectic structures has recently been underscored by Tiller (1), Chadwick (13) and Winegard and co-workers (11,14-16) on eutectic growth. Tiller suggested a mechanism applicable to lamellar eutectics with isothermal solidification interfaces for the transition of the morphology from lamellar to rod-like to globular. He proposed that a transition occurred when differences in supercooling between lamellae were created either by increased solute or freezing rate (1). If a ternary addition had a substantially different distribution coefficient or K value in the two phases of a binary eutectic, a difference in the constitutional supercooling in advance of the lamellae of each phase would develope during solidification. The phase with the smaller K value would lag, since it had the greater supercooling in front of it. As solidification progressed, local protuberances would occur on the interface of the lagging phase, grow rapidly out into the area of high supercooling, thus relieve some of the supercooling in front of the rest of this phase. The leading phase could then overgrow these

"relieved" areas of the lagging phase and a rod-like morphology for the sub-ordinate phase result. Chadwick has analyzed this aspect of the transition in detail (13). Tiller proposed further that with even greater differences of supercooling in front of each of the two phases, the leading phase could completely overgrow the lagging phase, thus a particulate distribution of the subordinate phase would result.

Recently Winegard and co-workers (14-16) have developed an argument based on constitutional supercooling to account for the majority of observed eutectic structures. If the K value for the two phases in a binary eutectic are substantially different, the phase with a low solute K value will tend to assume a morphology consistent with the large undercooling in front of it, while the phase with the higher K value will grow with a planar interface. Thus silicon, which has a very low solute K value, will assume a dendritic morphology and aluminum will lag with a planar interface. This explains their findings that silicon is continuous throughout a eutectic cell in either slowly or rapidly cooled alloys. Thus, the change in microstructure with cooling rate really reflects the change in cell size, and an increase in the number and fineness of the dendritic arms.

B) Structure Refinement

Refinement of as-cast structure can be achieved to varying degrees by such techniques as rapid cooling, vibrations, moving electro-magnetic fields and small alloying additions. Generally,the resulting change in structure improves one or more properties of the as-cast material. Of the methods available, the use of alloying additions is the most useful for commercial casting (17). The other methods either cannot be easily adapted or prove to be limited due to specimen size for successful commercial applications. Only the influence of alloying will be considered in the following discussion.

Refinement resulting from alloy additions must be considered in terms of both nucleation and growth phenomena (17-23). Additions of certain elements or compounds refine the as-cast structure by providing stable, effective nucleation sites (inoculation) and/or restrict grain growth through constitutional supercooling. An inoculant can be formed in the melt by chemical reaction before general solidification starts (17) or it can be added to the melt during casting (18) or it can be included in the mold wash on the cavity and core surfaces (20). The importance of nucleating effects on cast structure was demonstrated by recent work on high strength

steel castings (18). A completely columnar structure was replaced by an equiaxed structure when two cylinders were cast under identical conditions except the equiaxed specimen had a small amount of titanium added. In this situation independent nucleation was a major influence in determining the as-cast structure. The titanium addition also influenced the microstructure of the alloy by reducing the secondary arm spacing of the dendrites.

This latter refinement of morphology is generally considered a growth phenomenon controlled by constitutional supercooling at the liquid-solid interface (21-23,25). It is characterized not only by a reduction in the secondary arm spacing, but also by an increase in the complexity of the dendrite morphology with the appearance of tertiary and higher order arms. Alexander and Rhines (24) in their study of dendrite solidification, using high purity binary alloys determined: (a) dendrite arm spacing and grain size were independent within limits and (b) dendrite spacing was inverse to the solidification rate. More recent work by Spear and Gardner (21) using four commercial aluminum alloys was in general agreement with these results. The independence of grain size and dendrite arm spacing is caused by the dependence of dendritic growth on the rate of solidification while grain

size is a function of both nucleation frequency and growth condition. In the work on the aluminum alloys, it was determined that the as cast grain structure was determined as soon as the alloys had cooled a degree or two below the liquidus, even if the dendrite arm spacing changed an order of magnitude within a grain because of changes in freezing rate.

Howarth and Mondalfo (25) found from work with aluminum-copper alloys that the rate of cooling was more important than the rate of advance of the solidifying interface in determining dendrite spacing. The structure was refined as cooling rate increased for a given alloy composition. They also observed that dendrite spacing decreased as the alloy content approached the eutectic composition from either the hypo- or hypereutectic regions. It was concluded that the dendrite structure was diffusion rather than heat transfer controlled, emphasizing that the nature of the diffusion boundary layer about the dendrite determined the spacing. It has been observed (21-23) that lower degrees of solid solubility of the solute (i.e. rejecting more solute at the solidifying interface) produce greater growth along primary arms, a more complex dendrite structure and more columnar grains. These observations also emphasize the importance of the diffusion boundary

layer in the determination of dendritic structures.

C)  Directional Solidification:

Directional solidification is a technique which has been developed extensively in the last decade to control the macrostructure of a casting by control of the thermal conditions of solidification.  A steep thermal gradient is created in the melt through use of such devices as chills and auxiliary heating of the mold to produce uni-directional solidification.  Under some conditions a uniform rate of solidification is also approached.  In this manner, the grain structure is aligned with the direction of heat flow, the feeding of the casting is improved and the dendritic structure is more uniform (28).

Structure and Properties:

In general, a change in cast structure will be reflected in variations in one or more properties of the cast alloy.  For example, modification of an aluminum-silicon alloy will usually increase both the ultimate tensile strength and percent elongation (5).  The beneficial effect of refining the cast structure of a material is reflected by the increases in both tensile strength and ductility of refined alloys (17).  Though, normally, structural refinement is associated with a joint refinement of the grain size and dendrite spacing, the work of

Brown and Adams (22) indicates that the refinement in some situations of the dendrites has more influence on mechanical properties than grain size effects these. Other beneficial effects attributed to grain refinement have been a decreased tendency to hot tear and an increase in pressure tightness (26). Commercially, grain refinement is practiced with a variety of cast metals, such as, aluminum, magnesium and copper alloys and eutectic cell size of gray iron, with beneficial results on properties (17).

The advantages of directional solidification are reported to be the production of more sound castings with less microporosity, improved composition homogeneity (28,29) and a resulting improvement in yield strength and elongation. However, the improvement in properties may result more from the solidification conditions with a steep thermal gradient at the liquid-solid interface (18) than from the structure per se.

Until now, this discussion has been limited to room temperature properties, yet many of the structure characteristics discussed previously should provide improved high temperature properties. One of the major mechanisms for strengthening at high temperatures is the dispersion of a second phase as fine hard particles

randomly throughout the softer matrix.(29)   To be

effective, these particles should be strong, hard, stable

and resistant to agglomeration at elevated operating

temperatures.   Generally, the hardening phases are re-

fractory compounds, e.g. carbides, nitrides, etc., or

intermetallics.   The dispersion of the particles in the

matrix is also critical.   It has been shown that the

strength and resistance to creep at elevated temperatures

increases with the uniformity of the dispersion, smaller

size of the particle and a shorter mean-free path between

particles (28-31).

A precipitation-hardened material is limited to an

operating temperature below its solution temperature,

generally of the order of 0.5-0.6 of the melting point of

the matrix, whereas the phases in a eutectic coexist to

its melting point.  Therefore,  if the subordinate phase

of the eutectic could be "modified" sufficiently, a stable

dispersion of fine, hard particles would result in the

as-cast structure.   The modification of the eutectic

should also improve ductility without loss of strength by

changing the shape of the subordinate phase particles

from a plate-like or elongated dimension to a more rounded,

equiaxed type or at least with a reduced length in any

direction in the matrix.   The refinement of the dendritic

structure, with resulting refinement of inter-dendritic constituents, should also improve high temperature properties, by creating a more random dispersion, and a shorter mean free path between particles.

Purpose:

The purpose of this investigation was threefold: first, to utilize the techniques and theories of eutectic modification and structure refinement to obtain improvements in the properties of superalloys over those currently obtained with cast Ni-W and Co-W alloys; second, to establish criteria for the development of the desired as-cast structures; and third, to correlate variations in the as-cast structure with high temperature properties.

EXPERIMENTAL PROCEDURE

Alloys Investigated:

On the basis of previous work (2), two alloy systems, Ni-W and Co-W, were chosen for study, since these provided the best properties and response to modification. The Ni-45W and Co-45W forms the eutectic alloy in each system (33). All alloys were cast as test bars for stress rupture and tensile testing. Initially, two series of test bar clusters were cast for each of the alloy systems studied. Four compositions were chosen from each system (Ni-W and Co-W) so that one solid solution alloy

(-35W), one hypoeotectic alloy (-40W), one eutectic alloy
(-45W) and one hypereutectic alloy (-50W) were included.
One series of tests for each composition was unmodified;
another series was modified by a single addition of 0.75%Zr,
0.75% Ti, 0.3%C and 0.1%B. This relatively large and com-
plex mixture of alloying elements was chosen to insure con-
siderable modification at the start of the work.

As a result of stress-rupture tests of these alloys at
1800°F, the Co-35W alloy was selected as the base compo-
sition for further study and development. A series of
alloys were cast to determine the influences of known solid
solution strengtheners such as Cr, Mo and carbide formers
and structure modifiers such as Ta, Cb, Ti, Zr V, (31,32).
Additions were of the order of 1-3 weight percent; these
were added both singularly and in combinations. A number
of heats of an alloy of composition Co-35W-3Cr-1Ti-1Zr-.5C-
.1B were also employed to determine the influence of vari-
ations in the melting and casting procedure on structure
and properties. A third series of alloys to determine the
specific influence of Ti, Zr and C additions on the cast
structure and properties of a Co-35W-3Cr base alloy has
been cast, but not as yet evaluated. A complete list of
the alloys cast is shown in Table I.

A few representative castings were selected for wet chemical analyses by an independent laboratory. X-ray fluorescence analysis for Co was performed at Case as a quality control procedure, and was accurate to $\pm$ 0.2 weight percent. The X-ray technique was also used to determine Co variations within the castings. Specimens were cut and analyzed from top and bottom portions of both test specimens and sprue areas.

Melting and Casting Materials and Technique:

The melting stock was high purity material of the form and analysis listed in Table II. Representative heats were analyzed to determine the recovery of the various elements. Ceramic shell molds with a slip coat refractory of zircon made by the lost wax process were used for casting test bar clusters. Dewaxed shell molds were maintained at temperature in the vacuum chamber by a small resistance furnace. Figure 1 shows a shell mold and a cluster of test bars cast from a mold.

A 250-KW, 960 cps induction unit was used for melting. A modified vacuum melting procedure was necessitated by the use of thin-walled stabilized zirconia crucibles surrounded by a graphite susceptor. The melting procedure was started by placing a crucible packed with all of the charge except approximately 30 percent of the Ni or Co and

any oxidizable additions such as Ti or Zr in the
graphite susceptor. The additional charge metal was
loaded into a multicompartment chamber and the shell
mold placed in the mold heating furnace. The vacuum
chamber was then pumped down to a pressure less than 5
microns of mercury. While the chamber was being evacuat-
ed, a very low power was applied to the induction coil.
The charge was heated to 300-400°F in order to drive off
any absorbed water, as a precaution against cracking of
the crucible during melt down. When the chamber was
evacuated, power was slowly increased until the charge
started to melt (about 30 minutes). The chamber was then
back-filled with dry argon to 15 inches of mercury pressure.
The additional Ni or Co was added, the entire charge mel-
ted and superheated about 100°F (optical) above the melt-
ing temperature.

A vigorous boil without spitting was initiated at
this point and continued for approximately 20 minutes.
Following the boil, the chamber was again back-filled to
15 inches of mercury and the melt superheated approxi-
mately 350-400°F (optical) to insure dissolving of the
tungsten. At peak temperature, the oxidizable elements
such as titanium and zirconium were added and the temper-
ature immediately lowered 50-100°F (optical) and the melt

cast. The molds were left in the vacuum chamber for one hour after casting. The power to the mold furnace was cut immediately after the casting was poured. Then the molds were removed and the test bar castings shaken out. The test bars were cut from the sprue, sand blasted, and their surface inspected visually with a binocular microscope.

Several heats of Co-35W base alloys were cooled after the superheat until solidification occurred to determine freezing temperatures. The freezing temperature was read by means of an optical pyrometer and used as a reference point for establishing superheat and pouring temperatures. Thus, in subsequent discussions these temperatures are listed as a specific number of degrees above the freezing temperature of the alloy. A 100°F temperature change, as measured optically through a prism and 1/4 inch thick pyrex sight glass, was equivalent to approximately 125°F actual temperature as determined with a Pt-Pt+10% Rh thermocouple.

Metallographic and Mechanical Property Determinations :

Sections were cut from the gage length portion and button head of both as-cast and tested stress-rupture bars for metallographic examination. Cobalt-base alloys were etched using either concentrated hydrochloric acid with a

few drops of hydrogen peroxide or a modified Fry's etch
with 50 parts hydrochloric acid, 25 parts nitric acid,
1 gram cupric chloride and 150 parts water. Nickel-base
alloys were etched using either the hydrochloric-hydrogen
peroxide combination, or electrolytically with 10% oxalic
acid in water. The phases observed were generally not
identified by means other than metallography. It was
assumed that the phases that combined to form in the un-
modified binary alloys were defined by Hansen (33). Most
of the microconstituents of the multi-element alloys have
been described in the literature (35,36). A limited
amount of phase extraction work was performed and, in
general, served to confirm the identification of phases
already estimated on examining the microstructures op-
tically.

Macro-grain size was obtained by deep-etching with
either of the cobalt-base alloy etchants listed above.
The mean free path between microconstituents was deter-
mined using a line-point intercept method (34). Mean
free paths were usually measured on unetched specimens,
observing the surfaces optically at 250 magnifications
with a binocular microscope equipped with a filar eye-
piece.

Stress rupture testing was conducted with as-cast,
cast-to-size test bars. The test bars employed, as shown

in Figure 1, had a gage length of 1.250 inches and were

0.250 inch in diameter (37). All stress rupture tests were

performed in air at 1800 and 1850°F.

## RESULTS AND DISCUSSION

The results and discussion of this investigation are

presented in two parts. Part I deals with the initial

phase of the study during which a survey of the Co-W and

Ni-W systems was completed. Part II is concerned with

the subsequent study of modification and refinement of

Co-35W base alloys and the correlation of as-cast structure

with high-temperature properties.


Part I

Chemical Analysis:

A few representative castings were selected for wet

chemical analysis by an independent laboratory. These

results, with the charged compositions, are presented in

Table III. While almost all of the tungsten was recovered

in the binary alloys, a definite tungsten loss occurred in

the more complex alloys. This loss was consistently 1-1.5

weight percent tungsten as indicated by both wet chemical

analysis and X-ray fluorescence analyses. The reason for

the W loss was not determined. Variation between different

areas of the casting did not follow any pattern and was no

greater than 0.5 percent. Therefore, settling of tungsten-

rich phases from gravity was not a problem. The re-
coveries of the other elements checked, Ti, Zr, C and B,
were generally very high. Accordingly, the charged compo-
sitions were used for the following discussion.

Survey of Ni-W and Co-W Systems:

The initial portion of this investigation was con-
cerned with a survey of the Ni-W and Co-W systems, both
with unmodified binary compositions and a single addition
of several modifying elements to each of the binary alloys.

The structures of the unmodified and modified alloys
are indicated in Figures 2 through 5. Figures 2 and 3
show the structure for the Ni-35W, Ni-40W, Ni-45W, and
Ni-50W, while Figures 4 and 5 illustrate the micro-
structure for Co-35W, Co-40W, Co-45W, and Co-50W.

The structures of the binary alloys investigated,
except for the Co-50W, were modified markedly by the
combination additions of Ti,Zr, C and B. The lamellar
types of eutectic structures were replaced, for the most
part, by a globular carbide with only minor amounts of
fine eutectic dispersed along the grain boundaries. The
modified structures appear more columnar in form and
contained dendrites that were clearly outlined by carbides
and small eutectic islands.

The unmodified alloy of the Co-35W composition had an

equiaxed grain structure with a Widmanstatten precipitate of $Co_3W$ in the grain boundaries (38): the Ni-35W alloy had even a larger grained equiaxed structure without a grain boundary precipitate. Modification changed both alloys to a columnar structure with islands of carbides and eutectic dispersed discontinuously in the interdendritic areas. The unmodified Co-40 and Ni-40W alloys exhibited an equiaxed structure with a thin layer of eutectic at the grain boundary. This structure was modified to a columnar type with globular carbides and small islands of fine eutectic outlining the dendrites. The distribution of the carbides and eutectic was noticeably finer for the cobalt than nickel alloys for both 35 and 40W. This reflects the considerably lower solubility of carbides in cobalt than in nickel (39).

The unmodified Co-45W was almost totally eutectic, while the Ni-45W had considerable primary nickel, despite the fact that the equilibrium diagram indicates that both are eutectic compositions. Modification of the Co-45W resulted in thick platelets of the intermetallic $W_3Co_3C$ or $\eta$ phase as well as globular monocarbides (36). The modified Ni-45W contained a considerable amount of carbides both in massive globular form and as more angular "chinese script". Modification completely

eliminated the lamellar eutectic that occurred in the unmodified eutectic alloys.

The unmodified structures and the influence of modification on the Ni-50W and Co-50W differed appreciably. The Ni-50W unmodified structure contained both primary nickel and rounded or star-shaped primary tungsten with some areas of fine eutectic. Modification replaced the eutectic with coarse angular carbides. The amounts of primary nickel were increased and primary tungsten decreased by this modification. The unmodified Co-50W had a large grained lamellar eutectic structure of alternate platelets of $\eta$ phase and primary cobalt. Modification coarsened the lamellar structure markedly without appearing to alter the phases. The primary cobalt appears to contain a Widmanstatten precipitate, possibly the peritectoid reaction product, $Co_3W$.

The stress-rupture properties of this series of alloys are presented in Table VI and are plotted in Figure 6. In general, modification of the structure resulted in a ten fold or greater increase in time to fracture and considerable improvement in ductility at 1800°F. Percent reduction in area is considered a better indication of ductility than percent elongation after stress-rupture testing, since falsely high results in elongation are

produced by the cracks and voids formed during the later portion of the test. The modified Co-W alloys provided the largest increase in properties and the longest times to fracture of the alloys studied. Modification of Co-40W alloy increased the time to fracture at 1800°F a maximum of from 0.9 hour to 80 hours at an initial stress of 15,000 psi. The reduction in area increased from 1 to 22.8%. The stress-rupture properties at 1800°F of the Co-35W were increased from 6-7 hour life at 15,000 psi for the unmodified alloy to 52 hours at 15,000 psi in the modified condition; the reduction in area was also improved from 1 to over 90%.

With modification, the Co-45W alloy increased the time to fracture from 1-2 hours at 10,000 psi to 40.5 hours at 15,000 psi. Both the modified and unmodified alloys were brittle with approximately 1% reduction in area. The unmodified Co-50W was brittle with a stress rupture life of 3.5-7.3 hours at 10,000 psi. The coarse platelets of $\eta$ phase in the lamellar structure of the modified Co-50W, as illustrated in Figure 5d, were so embrittling that a sound casting could not be obtained.

The Ni-W alloys tended to be brittle in the unmodified condition with times to fracture of only 1-4 hours at 15,000 psi at 1800°F. Modification increased both the

time to fracture and the ductility of these alloys. The modified Ni-35W alloy increased in life from less than 1 hour to 15.8 hours at 15,000 psi at 1800°F. The unmodified alloy failed transgranularly with nil ductility; the modified alloy failed in a ductile manner with reduction in area of approximately 70%. The time to fracture at 15,000 psi for the Ni-40W alloys was increased from 1 hour to 9 hours by modification and the reduction in area increased from less than 1% to approximately 33%.

The unmodified Ni-45W and Ni-50W were brittle and weak and fractured after 1-5 hours at 15,000 psi and 1800°F Modification improved both alloys, increasing time to fracture to 13 hours at 15,000 psi for the Ni-45W alloy and to approximately 40 hours for the Ni-50W. The ductility of both alloys increased from less than 1% to about 6%.

The stress rupture curve for one of the best NASA experimental Co-base superalloys (42) at 1850°F was included in Figure 6 for comparison and as an indication of the relative behavior of these initial alloys compared to commercial superalloys of similar type. Both the modified Co-35W and Co-40W compared favorably to the Co-base superalloy, whereas none of the Ni-W alloys approached the desired strength levels.

Increasing the testing temperature from the 1800°F

used on the first series of tests to 1850°F for subse-

quent measurements causes a significant lowering of the

stress-rupture properties for a given alloy. For example,

the life of the modified Co-35W alloy was 52.2 hours at

15,000 psi and 1800°F and only 34.9 hours for the same

initial stress at 1850°F. The poorer properties of the

Ni-W alloys were even more significant since nickel-base

superalloys generally have a 10 to 20,000 psi advantage

over Co-base alloys for 100 hour time to fracture at this

temperature range (43). In view of their poor performance,

further study of the Ni-W system was stopped. Though the

Co-40W alloy had the best stress rupture properties of

the modified alloys tested, it was decided on the basis

of strength-to-density ratio that the Co-35W held more

promise. Accordingly, this composition served as the

base for all subsequent alloys investigated.


Part II

Structure Modification and Refinement of Co-35W Base Alloys :

A series of Co-35W base alloys were cast to investi-

gate the influence of both solid solution strengtheners

(Cr and Mo) and the carbide formers and grain refiners

(Ti,Zr, V, Ta and Nb) on structure and properties. The

selection of these alloys was based partly on previous work on Co-W alloys (32,40-42).

Representative microstructures of both the as-cast and"after-testing" structures are illustrated in Figures 7-16. The structure of the alloys etches more readily after testing and for this reason these structures appear darker. Photomicrographs marked "after-testing" are of samples cut from the gage length of specimens tested in air at 1850°F and 20,000 psi initial load. A series of heats of the same composition (Co-35W-3Cr-1Ti-1Zr-0.5C-0.1B) was cast to determine the influence of variations in casting procedure on structure and properties. Figures 17 and 18 show the macrostructure and micro-structure respectively of these heats.

By increasing the Ti, Zr, and C levels from those used in the original modification of Co-35W, as shown in Figure 7, the dendritic structure was refined and the microconstituents further modified and refined (see Figure 8). The eutectic areas in the original alloy were mostly eliminated and the elongated $\eta$ phase particles further divided. A slight change in the etching character-istics of the as-cast matrix occurred, which probably indicates some influence of the increased alloying on the peritectoid reaction (40). No significant difference

occurred in the as-cast grain size; this was about 2-5 grains per 1/4 inch diameter cross-section in the gage length for these two alloys. After testing at 1850°F, both samples show heavy precipitation of the $Co_3W$ phase. The eutectic islands of the Co-35W-0.8Ti-0.8Zr-0.2C-0.1B appear to have partially agglomerated to form solid particles of the $\eta$ phase. Otherwise, the structures of both alloys are unchanged after testing.

The addition of 3% Cr as a solid solution strengthener was suggested by the work of Freche et al (41) on Co-25W base alloys. Some changes in microstructure occurred that were primarily minor refinements of the dendritic structure, shown in Figures 9 and 10, and the loss of most of the matrix precipitate in the as-cast material. The grain size of these alloys was approximately 8-10 grains per 1/4 inch diameter cross-section in the gage length. This was a decrease from that of the alloys with no chromium of comparable Ti, Zr and C levels. The 3% Cr alloys showed the same microstructural changes after testing as the alloys with no chromium; heavy precipitation of $Co_3W$ and little change in the morphology or distribution of the carbide phases occurred.

The change in microconstituent morphology and size with increasing Ti and Zr content was very minor in the

3% Cr alloys in comparison with the observed change in
the alloys without Cr. This may indicate more influence
of C at the 0.5 percent level than of Ti and Zr on the
structure of these alloys for both 3% Cr alloys. This
influence of C is also indicated by comparing Figures 7
and 9. Ti and Zr levels are similar in these alloys
whereas C levels differ from 0.2 to 0.5%. The volume of
microconstituents has increased and the particles are
generally finer, less elongated at the higher C level.

The effect of increasing Ti, Zr and C further to
obtain a composition of Co-35W-3Cr-2Ti-2Zr-1C-0.1B is
illustrated in Figure 11. The structure appears random,
with large idiomorphic carbide particles and small islands
of carbide eutectic. The particle distribution nearly
obscures all indications of the dendritic morphology and
as-cast grain structure. The grain size of the alloy was
3-4 grains per 1/4 inch diameter cross-section in the gage
length and appreciably coarser than the other 3% Cr alloys.
After testing at 1850°F, the $Co_3W$ precipitation of this
alloy was considerably coarser than in previously discussed
alloys, while the distribution and morphology of the micro-
constituents was unchanged. The heavy matrix precipi-
tation is probably caused by the longer time at elevated
temperatures experienced by these alloys.

The addition of B has been shown to change the morphology of grain boundary carbides in many commercial superalloys (31). This influence is emphasized by the structure shown in Figure 12. When B was not added to a Co-35W-3Cr-1Ti-1Zr-0.5C alloy, the morphology of the complex carbide ($\eta$ phase) partially reverted to its unmodified, lamellar form. Comparing the as-cast structures in Figures 10 and 12, it appears that the $\eta$ phase was particulate in the alloy with B but has collected at the grain boundaries as a semi-continuous, embrittling film in the alloy without B.

Since the Co-W and Co-Mo phase diagrams are very similar, an alloy with part of the W replaced by Mo on an atomic basis was investigated. The molybdenum may replace the W in solid solution and provide some further solid solution strengthening of the matrix. Since the strength-to-weight ratio is a critical factor in the usefulness of any high temperature alloy, the replacement of a heavy element (W) with a lighter one (Mo) could result in a substantial improvement for similar or improved high temperature properties. Figure 13 illustrates the microstructure of an alloy where 2.6 percent Mo was substituted for 5 percent W (i.e. equal atomic amounts). The carbides in this alloy were considerably more

irregular, and a very fine, less than 1 μ diameter, randomly-dispersed phase appeared. Generally, the amount of the complex carbide phase appears to have increased with the Mo addition, while the smaller, more spherical, monocarbide phase decreased. After testing, the structure of the carbide phases showed more change than in the standard alloy. For purposes of subsequent discussion, the Co-35W-3Cr-1Ti-1Zr-0.5C-0.1B alloy shown in Figure 10 will be referred to as the "standard alloy". The complex carbide was elongated and interconnected; the matrix precipitate was very coarse and the new phase has apparently been completely dissolved.

Additions of V and Nb plus Ta to the standard alloy were investigated to determine the influence of multiple carbide formers. Comparing the as-cast structures in Figures 10 and 14, it is noted that the addition of 1% V has slightly altered the as-cast structure by coarsening carbide particles. After testing it was observed that the complex carbide phase had agglomerated partially and the matrix precipitate was very coarse. The oxidation rate during testing of the 1% V alloys was also considerably greater than that of the standard alloy. The effect of the addition of 1% Nb plus 2% Ta is shown in Figure 15. A new carbide phase has formed, the microconstituents are

generally elongated, enlarged and have a very irregular
shape. The carbide structure was reasonably stable
during testing while the matrix precipitate was coarser
than observed in the standard alloy.

Nitrogen as CrN powder was added to the standard
alloy in an attempt to refine the microconstituents. The
powder was wrapped in pure Ni foil and plunged after the
Ti and Zr addition. Both the macro- and microstructure
was coarsened by this treatment as illustrated in Figure
16. The complex carbide phase reverted back to its
elongated, broken lamellar structure and areas of eutectic
formed along the sides of the coarse carbide particles.
A small amount of very fine new phase, similar to that in
the Mo modified structure, occurred in the as-cast
structure. After testing, the broken lamellar pattern of
the microconstituents is very apparent, and the matrix
precipitate is again coarser than the standard alloy.

A series of four heats of the standard alloy were
cast with various pouring conditions to determine the
sensitivity of the as-cast structure and high temperature
properties to casting procedure. The following table
summarizes the pouring conditions used:

| Casting | Superheat (Optical) °F | Superheat for Pouring (Optical)°F | Mold (Thermocouple)°F |
|---------|------------------------|-----------------------------------|-----------------------|
| A | 400 | 300 | 1600 |
| B | 400 | 200 | 1600 |
| C | 300 | 300 | 1600 |
| D | 400 | 300 | 1300 |

Representative macro-and microstructures are illustrated in Figures 17 and 18.

The macrograin size varied some with pouring temperature and superheat, as shown in Figure 17. The higher superheat and pouring temperatures for casting A resulted in a larger grain size than for either the lower superheat of casting B or the same superheat with lower pouring temperature of casting C. The temperature of the investment mold was observed to have more of an influence since the smallest grain size was produced when the mold temperature was reduced from 1600°F to 1300°F for casting D. The representative structures illustrated in Figure 18 indicate that only minor variations in structure were obtained among the four castings.

Mechanical Properties of Co-35W Base Alloys:

The influence of Ti, Zr, C and Cr on the stress rupture life of the base Co-35W alloy at 1850°F is shown in Figure 19; the influence of Mo, V, N and Ta+ Nb

additions on the standard (Co-35W-3Cr-1Ti-1Zr-0.5C-0.1B) alloy is presented in Figure 20; and the effect of variations in casting procedure is shown in Figure 22. Tables V and VI list both time to fracture and reduction in area at the different levels of initial stress. After some tests, the calculation of reduction in area was questionable due either to the anistropic nature of the fracture cross-section or extensive oxidation of the test specimen. These values have been marked either (a) or (o) in Tables V and VI.

The data in Figure 19 indicates that higher Ti, Zr, and C levels of a base Co-35W-3Cr alloy substantially increases the stress-rupture life at 1850°F. An increase from 0.8Ti-0.8 Zr-0.5C to 2Ti-2Zr-1C more than tripled (from 63.5 hours to 224.9 hours) the time to fracture at 15,000 psi,while retaining the ductility (reductions in area of approximately 30 percent). This latter alloy and the Co-35W-3Cr-1Ti-1Zr-0.5C-0.1B alloy had better stress rupture properties at 1850°F than one of the best Co-base superalloys reported in the literature, an experimental NASA alloy (42). The stress rupture curve for the NASA alloy is plotted for comparison in Figures 19 and 20. A more detailed study of the separate effect of each element, and their interaction effects on structure and

high temperature properties is now in progress.

The effect of the 3% Cr addition was not as marked as the changes produced by Ti, Zr, C but was substantial at the lower stress levels. The time to fracture at 15,000 psi was increased from 110 hours without Cr to 145 hours with 3% Cr. This improvement appeared to result from a retardation of the precipitation of the $Co_3W$ phase by the Cr, as indicated by the heavier, coarser matrix precipitation illustrated in Figure 8-D compared to the alloy with 3% Cr (Figure 10-D) and a moderate refinement of the structure.

Embrittlement of the standard alloy resulted without boron, as indicated by the data in Figure 12 and Tables V and VI. The stress-rupture curve of the alloy with no boron additions was drastically lowered. The time to fracture at 15,000 psi and 1850°F was decreased from 145 to 52 hours without boron. The loss in ductility is even more marked; the reduction of area decreased from 20-50% with boron to low ductility (4-8%) without boron.

No further improvement in properties was obtained by the addition of Mo, V, Ta + Nb or N, as illustrated in Figure 20. In fact, the properties of all these alloys were substantially below those for the standard composition. The standard composition was the only alloy with comparable

properties to the NASA alloy. All specimens failed by
intergranular rupture. The initiation of voids and cracks
which cause intergranular failure at elevated temperatures
is directly related to the amount of grain boundary sliding
that occurs (46). As sliding increases, the number and
size of the voids and cracks increase, and the creep re-
sistance of the material decreases. The various additions
influenced the grain boundary sliding of the alloys, as
indicated by the variation in surface roughening after
testing (Figure 21). The standard alloy showed only minor
slip outside of the immediate area of failure. In some
of the lower stress, longer time tests of this alloy,
cracking was observed away from the fracture area, and in
these regions localized grain boundary slip was observed.
The Mo addition caused extensive slip to occur the full
length of the gage section. The V addition greatly accel-
erated the oxidation of the alloy, practically obscuring
any surface roughening. However, judging by the generally
uneven surface, with several severely necked-down areas.
V also accelerated grain boundary sliding. Some surface
roughening occurred along the gage length of the alloy
with Ta plus Nb added, but the major deformation was
limited to the immediate area of fracture. N was observed
to have more of an influence on macro-grain size, than

grain boundary sliding since only localized necking with subsequent roughening and cracking in the immediate area of failure occurred on these alloys. The number of grains for the alloy was increased to 30-35 grains per 1/4 inch diameter from the usually 8-12 grains in the other alloys tested.

The temperature dependence of stress-rupture properties is reflected in the substantial increase in life when two of the alloys, Co-32W-2.6Mo-3Cr-1Ti-1Zr-0.5C-0.1B and Co-35W-3Cr-1Ti-1Zr-0.5C-0.1B were tested at 1800°F. These data are listed in Tables V and VI. The time to fracture of the alloy with Mo increased from 88.1 hours at 1850°F to 219.2 hours at 1800°F for an initial stress of 15,000 psi. Similarly for the standard alloy, Co-35W-3Cr-1Ti-1Zr-0.5C-0.1B, the time to fracture increased from 31.5 hours at 1850°F to 82.2 hours at 1800°F for an initial stress of 20,000 psi.

The alterations in the pouring conditions produced about a 10% increase in the scatter of the test results for this composition as shown in Figure 22. The decrease in time to fracture for casting B with a 200°F (optical) pouring temperature may be an indication of the slight coarsening of the microstructure and the resulting minor increase in the mean-free path between microconstituents.

However, the variation is small and slight variations in composition may cause more influence on properties and structure than moderate changes in the pouring procedure. The insensitivity of this alloy to changes in casting conditions has certain commercial advantages since it increases process flexibility. The greater the variation in allowable casting conditions, the greater tolerance that exists for process variables.

Relating Microstructure to High Temperature Properties :

Quantitative metallography was carried out on a number of the Co-35W base alloys to determine more specifically the changes in structure with variations in alloy content. The measured mean free path between microconstituents and the macrograin size are listed in Table VII. Figure 23 presents a graph of spacing versus time to fracture for specimens tested at 1850°F and 15,000 psi initial load.

As shown in Figure 23, a linear correlation between the logarithm of the mean free path and the logarithm of the stress rupture life was determined. The microconstituents normally fell into two groups: larger, irregularly shaped particles of the order of 5 micron by 10 micron mean dimensions, tentatively identified as the complex carbide or $\eta$ phase, and smaller, more regularly

faceted particles of the order of less than 1 to 5 microns,
identified as the (Ti,Zr) phase. The particle spacings,
as measured by the number of particles intercepting
random lines of known length, were of the order of 10-40
microns. These dimensions are an order of magnitude or
more, larger than those normally encountered in studies
of alloy strengthening by dispersion of hard second
phases in a soft matrix, such as work on Nickel-$Al_2O_3$
alloys (46).

The Al-Cu alloy system, where $Al_2Cu$ particles can be
formed in a variety of shapes and with varying spacings
by precipitation from solid solution through well es-
tablished heat-treatments, has been studied in some de-
tail (47). Though the particle spacings in these latter
studies were of the order of those found in this investi-
gation, only minimum or secondary creep rates were
correlated to spacing. It was found that the minimum
creep rate decreased as the spacing decreased; accordingly,
times to fracture should increase as the creep rate(and
spacing) decreased. As Garafalo (45) emphasizes, minimum
creep rate can only be correlated with stress rupture
life if the matrix remains stable throughout the test,
with no metallurgical changes such as recovery or phase
transformation. Normally if such changes take place,

failure occurs earlier than predicted by the secondary
creep rates. The correlation of spacing to stress
rupture life does suggest that at times microstructural
variations may have more influence than moderate vari-
ations in composition.

As noted previously, all the alloys tested failed
intergranularly. Thus, grain size and grain boundary
constituents are other factors to be considered in the
evaluation of the stress rupture test results. A larger
grained material would be expected to have longer stress
rupture life with all other factors held constant, since
the grain boundary area is reduced. An increase in the
number and decrease in the size of the grain boundary
constituents would increase life by providing more re-
sistance to grain boundary sliding. The influence of
grain structure could not be fully established on the
basis of the tests to date. The macrograin size varied
irregularly with increased alloy content as shown in
Table VII. Increasing the Ti, Zr and C levels increased
the volume percent of the carbide phases and refined the
microstructure. Consequently, more and finer particles
were created in the grain boundary areas, thus helping
to strengthen the alloy. The improved properties of the
Co-35W-3Cr-2Ti-2Zr-1C-0.1B alloy probably indicates the

combined influence of larger grain size and a greater volume percent and more uniform dispersion of the carbide phases.

## SUMMARY

From a survey of both the Ni-W and Co-W systems, it was shown that the majority of binary alloy structures could be successfully modified by a single addition of 0.75-Ti-0.75Zr-0.5C-0.1B. The modified alloys had substantially improved stress rupture lives and ductility. A Co-35W composition was chosen, on the basis of the improved properties of the modified alloy and strength to weight ratio considerations, for further investigation and development.

In subsequent alloying of the base Co-35W alloy, it was determined that additions of Ti, Zr, C and Cr refined and modified the base structure, thus imparting improved properties; Mo, V, Ta +Nb, and $N_2$, however, adversely influenced both structure and properties. Several of the alloys investigated had better stress rupture lives at 1850°F than the majority of commercially available cobalt-base superalloys.

Variations in casting procedure were found to have only minor influence on the structure and high temperature properties of a Co-35W-3Cr-1Ti-1Zr-0.5C-0.1B. Superheat,

pouring and mold temperatures were varied, causing some change in macrograin size and spacing of the microconstituents, but only adding about 10% to the scatter of the data for the stress rupture curve.

Generally, the improvement in properties was associated with a refinement of the dendritic structure and a change in the size and morphology of the microconstituents. A linear correlation between the logarithm of the microconstituent spacing and the logarithm of the time to fracture at constant stress and temperature was observed. The scatter encountered is believed to mainly reflect the influence of grain size variations.

## FUTURE WORK

A new series of Co-35W - 3Cr-0.1B base alloys with Ti, Zr and C levels varied according to a factorial design scheme has been cast but not evaluated to date. These alloys will be analyzed, not only to establish the individual and interaction effects of Ti, Zr and C on structure and properties, but also to furnish further information on the influence of structure refinement on properties. Limited microprobe analyses will be conducted to correlate compositional variations with changes in alloy content and structure refinement.

## List of References

1) Tiller, W.A.: The Modification of Eutectic Structure. Octa Met., vo 1.5, 1957, pp. 56-59.

2) Ashbrook, R.L. and Wallace, J.F.: Modification of Eutectic Alloys fcr High Temperature Service. Trans. A.I.M.E., vol. 236, 1966, pp. 670-678.

3) Chadwick, G.A.: Eutectic Alloy Solidification. Progress in Materials Science, vol. 12, No. 2, 1963.

4) Davis, V.de. and West, T.M.: Factors affecting the Modification of the Aluminum-Silicon Eutectic, J. Inst. Met., vol. 92, 1963-64, pp. 175-180.

5) Thall, B.M. and Chalmers, B.: Modification in Aluminum-Silicon Alloys. J. Inst. Met., vol. 77, 1950, pp. 79-97.

6) Kim, C.B. and Heine, R.W.: Fundamentals of Modification in the Aluminum-Silicon System. J. Inst. Met., vol. 92, 1963-64, pp. 367-376.

7) Schulz, E.: Microscopic Study of Grain Refinement of Silumin, Z. Metallkunde, vol. 39, 1948, pp. 123-128.

8) Kissling, R.J. and Wallace, J.F.: Refinement of Aluminum-Silicon Alloys. Foundry, May, 1963, pp. 142-151.

9) Mondolfo, L.F.: Eutectic Solidification, Discussion. J. Inst. Met., vol. 93, 1964-65, pp. 233-34.

10) Plumb, R.C. and Lewis, J.E.: The Modification of Aluminum-Silicon Alloys by Sodium. J. Inst. Met., vol. 86, 1957-58, pp. 393-400.

11) Bell, J.A.E. and Winegard, W.C.: Interconnection of Silicon in Modified Aluminum Silicon Eutectic. Nature, vol. 208, 1965, p. 177.

12) Meussner, R.A.: The Structure of Aluminum-Silicon Alloys. N.R.L. Report No. 5341, July, 1959.

13) Chadwick, G.A.: Modification of Lamellar Eutectic Structures. J. Inst. Met., vol. 91, 1962-63, pp.298-303.

14) Bell, J.A.E. and Winegard,W.C.:  Constitutional
    Undercooling and Growth of Eutectics. J. Inst. Met.,
    vol. 93, 1964-65, pp. 457-59.

15) Bell, J.A.E. and Winegard,W.C.:  Structure of Pure
    Aluminum-Silicon Eutectics. J. Inst. Met., vol. 93,
    1964-65,pp. 318-319.

16) Kerr, H. W., Bell, J.A.E. and Winegard, W.C.:
    Solidification of Binary and Ternary Eutectics.
    J. Australian Inst. Met., vol. 10, 1965,pp.64-69.

17) Wallace, J. F.:  Grain Refinement of Steels. J.
    Metals, May, 1963, pp. 372-376.

18) Church, N., Wieser, P. and Wallace, J.F.:  Control
    of Cast Grain Size of Steel Castings, Effect of
    Grain Refinement on Properties.  Trans. AFS.,Vol.74,
    1966, pp. 113-128.

19) Chalmers, B.: Principles of Solidification. John
    Wiley and Sons, New York, 1964.

20) Reynolds, J. A. and Tottle, C. R.:  The Nucleation
    of Cast Metals at the Mould Face. J. Inst. Met.,
    vol. 80, 1951-52, pp. 93.

21) Spear, R. E. and Gardner, G. R.:  Solidification of
    Aluminum Casting Alloys. Trans. AFS, vol. 68, 1960,p.36.

22) Brown, P. E. and Adams, C. M.:  Rapidly Solidified
    Alloy Structures,  Trans. AFS., Vol. 69,1961,p.879-91.

23) Form, G. W. and Wallace, J.F.:  Solidification of
    Metals, General Principles. Trans.AFS, vol. 68,1960,
    pp.145-56.

24) Alexander, B.H. and Rhines, F.N.:  Dendritic Crystal-
    lization of Alloys. Trans. AIME, vol.188,1950,
    pp. 1267-73.

25) Howarth, J. A. and Mondolfo, L.F.: Dendritic Growth.
    Acta Met., vol. 10, 1962, pp. 1037-1042.

26) Kissling, R. J. and Wallace, J.F.:  Grain Refinement
    of Aluminum Castings, Part 2.  Foundry, vol. 91,
    July 1963, pp. 45-49.

27) Poirier, D.R., Ebner, M.L., Fleming, M.C. and
    Backofen, W.A.: Effect of Processing History on
    Fracture of Materials at High Strength Levels.
    ASD-TDR-63-819, Part I, A.F. Materials Laboratory,
    Aeronautical Systems Division, Air Force Systems
    Command, Wright Patterson Air Force Base, Ohio.

28) Winegard, W.C.: Fundamentals of the Solidification
    of Metals, Met. Rev., vol. 6, No.21, 1961, pp.57.

29) Turkalo, A.M. and Low, J. R. Jr.: The Effect of
    Carbide Dispersion on the Strength of Tempered
    Martensite. Trans. AIME, vol. 212, 1958, pp.750-58.

30) Nutting, J. and Arrowsmith, J.M.: The Metallography
    of Creep-Resistant Alloys. Structural Processes in
    Creep, Spec. Rpt. No. 70, The Iron and Steel Insti-
    tute, 1961.

31) Wagner, H. J. and Hall, A.M.: The Physical Metallurgy
    of Cobalt-Base Superalloys. DMIC Rpt. 171, AF33(616)-
    7747, July 6, 1962, Columbus, Ohio.

32) Adkins, E. F., Williams, D. W. and Jaffee, R.I.:
    Development of Wrought Cobalt-Tungsten Base Alloys.
    Cobalt, vol. 8, Sept. 1960, pp. 16-29.

33) Hansen, M. and Anchenko, K.: Constitution of Binary
    Alloys, McGraw-Hill Book Co., Inc., New York, 1958.

34) Smith, C. W. and Guttman, L.: Measurement of In-
    ternal Boundaries in Three-Dimensional Structures by
    Random Sectioning. J. Metals, vol. 5, 1953, pp.81-87.

35) Felten, E. J. and Gregg, R.A.: The Physical Metallurgy
    and Oxidation Characteristics of a Cobalt-Base Super-
    alloy, SM-302. Trans. ASM, vol. 57, 1964, pp.804-22.

36) Rautala, P. and Norton, J. T.: Tungsten-Cobalt-
    Carbon System. Trans. A.I.M.E., vol. 194,1956,pp.
    1045-1050.

37) Freche, J.C. and Waters, W.J.: Exploratory Investigation of Advanced-Temperature Nickel-Base Alloys. NASA Memo 4-13-59E, May, 1959.

38) Toda, T.: On the Temper Hardening Properties of Cobalt-Tungsten Alloys, Trans. Jap. Inst. Met., vol. 6, July, 1965., pp.139-46.

39) Edwards, R. and Raine, T., as quoted in Schwarzkopl, P. and Kieffer, R.: Cemented Carbides. The Macmillan Co., New York, 1960, p. 71.

40.) Freche, J. C., Ashbrook, R. L. and Klima, S. J.: Cobalt-Base Superalloys for Space-Power Systems. J. Metals, 1963, pp. 928-34.

41) Freche, J. C., Ashbrook, R. L. and Sandrock, G.D.: High-Temperature, Cobalt-Tungsten Alloys for Aerospace Applications. J. of Engin. for Industry, Feb., 1965, pp. 9-20.

42) Freche, J. C., Ashbrook, R. L., and Sandrock, G.D.: The Potential for Cobalt-Tungsten Superalloys. Metals Progress, May, 1965, pp. 74-79.

43) Lund, C.H.: Physical Metallurgy of Nickel-Base Superalloys, DMIC Rpt. No. 153, AF 33(616)-7747, May 5, 1961 Columbus, Ohio.

44) Wheaton, H.L.: MAR-M-509,A New Cast Cobalt-Base Alloy for High Temperature Service. Cobalt, vol. 29, Dec., 1965, pp. 163-70.

45) Garofalo, F.: Fundamantals of Creep and Creep-Rupture in Metals. The Macmillan Co., New York,1965.

46) Cremens, W.S. and Grant, N.J.: Preparation and High-Temperature Properties of Nickel-$Al_2O_3$ Alloys. A.S.T.M. Proceedings, vol. 58, 1958, pp. 714-732.

47) Giedt, W. H., Shelby, D.D. and Dorn, J.E.: The Effect of Dispersions on Creep Properties of Aluminum-Copper Alloys. Trans. A.S.M.E., vol. 77, 1955, pp. 57-63.

TABLE I:  NOMINAL COMPOSITION OF ALLOYS INVESTIGATED
(weight percent)

Part I

Ni - 35W
Ni - 35W - .75Ti - .75Zr - .25C - .1B
Ni - 40W
Ni - 40W - .75Ti - .75Zr - .25C - .1B
Ni - 45W
Ni - 45W - .75Ti - .75Zr - .25C - .1B
Ni - 50W
Ni - 50W - .75Ti - .75Zr - .25C - .1B

Co - 35W
Co - 35W - .75Ti - .75Zr - .25C - .1B
Co - 40W
Co - 40W - .75Ti - .75Zr - .25C - .1B
Co - 45W
Co - 45W - .75Ti - .75Zr - .25C - .1B
Co - 50W
Co - 50W - .75Ti - .75Zr - .25C - .1B

Part II

Co - 35W - 1Ti - 1Zr - 0.5C - 0.1B
Co - 35W - 3Cr - .8Ti - .8Zr - 0.5C - 0.1B
Co - 35W - 3Cr - 1Ti - 1Zr - 0.5C - 0.1B
Co - 35W - 3Cr - 2Ti - 2Zr - 1.0C - 0.1B
Co - 35W - 3Cr - 1Ti - 1Zr - 0.5C

Co - 30W - 2.7Mo - 3Cr - 1Ti - 1Zr - 0.5C - 0.1B
Co - 35W - 3Cr - 1V - 1Ti - 1Zr - 0.5C - 0.1B
Co - 35W - 3Cr - 0.5Ti - 1Zr - 2Ta - 1Nb - 0.5C - 0.1B
Co - 35W - 3Cr - 1Ti - 1Zr - 0.5C - 0.1B - 0.1N
*
Co - 35W - 3Cr - 0.5C - 0.1B
Co - 35W - 3Cr - 2Ti - 0.5C - 0.1B
Co - 35W - 3Cr - 2Zr - 0.5C - 0.1B
Co - 35W - 3Cr - 2Ti - 2Zr - 0.5C - 0.1B
Co - 35W - 3Cr - 1C - 0.1B
Co - 35W - 3Cr - 2Ti - 1C - 0.1B
Co - 35W - 3Cr - 2Zr - 1C - 0.1B
Co - 35W - 3Cr - 2Ti - 2Zr - 1C - 0.1B


*This series has been cast, but not evaluated in time for
this report.

## Table II Melting Stock

| Element | Form | Purity |
|---|---|---|
| Boron | -325 mesh | 99.25 |
| Carbon | spectroscopic graphite | 99.999+ |
| Cerium | chips | 99.9 |
| Cobalt | electrolytic 1"x1"x1/8" | 99.5+ |
| Chromium | electrolytic | 99.8+ |
| Molybdenum | powder, 4 microns avg. | 99.0 |
| Niobium | -325 mesh | 99.0 |
| Nickel | electrolytic 1"x1"x1/8" | 99.9+ |
| Tantalum | roundels | 99.5 |
| Titanium | sponge · | 99.65 |
| Tungsten | powder, 6 microns avg. | 99.9+ |
| Vanadium | chips | 99.0 |
| Zirconium | sponge(reactor grade) | 99.8+ |

Table III    Chemical Analyses of Representative Heats

| Alloy Investigated Wt % | Analysis Wt % | | | | | | |
|---|---|---|---|---|---|---|---|
| | Co | W | Cr | Ti | Zr | C | B |
| Co-35W | 65.77 | Bal | | | | | |
| Co-40W | <0.75 | Bal | | | | | |
| Co-35W-.75Ti-.75Zr-.3C .1B | N.D. | N.D. | -- | 0.74 | 0.72 | 0.22 | 0.10 |
| Co-35W-3.2Cr-1Ti-1Zr-5C-.1B | 59.10 | N.D. | 3.15 | 1.04 | N.D. | 0.46 | 0.092 |
| Co-35W-3Cr-.8Ti-.8Zr-.5C-.1B | 61.50 | Bal | 2.96 | 0.79 | 0.76 | 0.48 | N.D |

N.D. - not determined-

# TABLE IV RESULTS OF STRESS RUPTURE TESTS IN AIR AT 1800°F.

| Alloy | Initial Stress, Psi | Time to Fracture Hours | Reduction in Area,% |
|---|---|---|---|
| **Ni-W Series:** | | | |
| Ni-35W -Unmod. | 15,000 | 0.9-1.4 | Nil |
| Ni-35W -Mod.(a) | 15,000 | 15.8 | 71.1 |
| | 20,000 | 0.9 | 36.7 |
| Ni-40W -Unmod. | 15,000 | 0.8-1.4 | <1 |
| Ni-40W -Mod.(a) | 15,000 | 8.2-9.1 | 32.4 |
| | 20,000 | 2.6 | 34.6 |
| Ni-45W -Unmod. | 15,000 | 1.5-4.0 | <1 |
| Ni-45W -Mod.(a) | 20,000 | 4.6 | 7.0 |
| | 15,000 | 12.7 | 6.2 |
| Ni-50W -Unmod. | 15,000 | 4.0-4.7 | <1 |
| Ni-50W -Mod.(a) | 15,000 | 38.9-40.4 | 3.1 |
| | 20,000 | 9.7-12.6 | 6.0 |
| **Co-W Series** | | | |
| Co-35W -Unmod. | 10,000 | 41.1-81.7 | <1 |
| | 15,000 | 6.3-6.7 | 1.2 |
| Co-35W -Mod.(b) | 15,000 | 52.2 | 94.2(c) |
| | 20,000 | 20.2-44.3 | 59.7 83.5(c) |
| | 25,000 | 5.3 | 79.4(c) |
| at 1850°F | 15,000 | 34.9 | 70.8(c) |
| Co-40W -Unmod. | 10,000 | 3.2-3.5 | <1 |
| | 15,000 | 0.9 | <1 |
| Co-40W-Mod.(b) | 15,000 | 78.7 | 17.2 |
| | 20,000 | 28.2-32.0 | 22.8 |
| | 25,000 | 12.2 | 32.0 |

a)  Additions Resulted in approximate composition of:
    0.7Zr, 0.5Ti, 0.2C, 0.1B

b)  Additions Resulted in Approximate composition of:
    0.7Zr, 0.7Ti, 0.2C, 0.1B.

c)  Anistropic deformation, assumed ellipsoidal
    fracture cross-section.

TABLE IV (cont)   STRESS-RUPTURE RESULTS

| Alloy | Initial Stress, Psi | Time to Fracture, Hours | Reduction in Area,% |
|---|---|---|---|
| Co-45W - Unmod. | 10,000 | 1.0-1.7 | <1 |
| Co-45W - Mod.(b) | 15,000 | 40.5 | 3.6 |
| Co-50W - Unmod.(b) | 10,000 | 3.5-7.3 | <1 |

(b)   Additions Resulted in Approximate composition of:
0.7Zr, 0.7Ti, 0.2C, 0.1B.

Table V   Results of Stress Rupture Tests in Air at
1850°F for Co-35W Base Alloys

| Alloy Composition (Nominal-Wgt. %) | Initial Stress Psi | Time to Fracture Hours | Reduction in Area Percent | |
|---|---|---|---|---|
| Co-35W-1Ti-1Zr-.5C-.1B | 15,000 | 110.7 | 42.5 | (A) |
| | 17,500 | 60.1 | 28.9 | |
| | 20,000 | 32.5 | 57.8 | |
| Co-35W-3Cr- 0.8Ti-0.8Zr .5C  -.1B | 15,000 | 63.5 | 21.3 | |
| | 20,000 | 23.2 | 30.0 | |
| | " | 27.6 | 18.9 | |
| | 25,000 | 9.8 | 27.2 | |
| | " | 8.3 | 62.5 | (A) |
| Co-35W-3Cr-1Ti-1Zr- .5C-.1B | 15,000 | 145.2 | -- (0) | Ave of 5 Heats |
| | 17,500 | 61.7 | -- | Heats Listed In-Dividually |
| | 20,000 | 29.5 | -- | Table VI |
| | 22,500 | 17.6 | -- | |
| | 25,000 | 11.5 | -- | |
| Co-35W-3Cr-2Ti-2Zr- 1C-.1B | 15,000 | 224.9 | 29.2 | (A)(0) |
| | 17,500 | 117.1 | 37.8 | |
| | 20,000 | 42.5 | 41.2 | (A) |
| | 25,000 | 14.9 | 28.9 | |
| Co-35W-3Cr-1Ti-1Zr-.5C | 15,000 | 52.0 | 7.0 | |
| | 17,500 | 29.8 | 2.5 | |
| | 20,000 | 20.4 | 4.8 | |
| | 25,000 | 8.0 | 8.7 | |
| Co-30W-2.7Mo-3Cr-1Ti- 1Zr-.5C-.1B | 15,000 | 88.1 | 43.2 | (0) |
| | 20,000 | 14.3 | 33.0 | (B) |
| | " | 16.6 | 22.0 | |
| | 25,000 | 7.6 | 48.5 | |
| | 15,000 | 219.2 | 25.2 | (0)tested-1800°F |

(A)   Anistropic deformation assumed, ellipsoidal fracture
      cross-section
(0)   Heavy oxidization

Table V (Continued)

| Alloy Composition | Initial Stress, Psi | Time to Fracture, Hours | Reduc. in Area, % | |
|---|---|---|---|---|
| Co-35W-3Cr-1Ti-1Zr-1V-.5C-.1B | 15,000 | 65.0 | 43.0 | (0) |
| | 17,500 | 42.8 | 22.0 | (0) |
| | 20,000 | 18.6 | 14.0 | (0) |
| | 25,000 | 7.0 | 33.4 | (0) |
| Co-35W-3Cr-0.5Ti-1Zr-2Ta-1Nb -0.5C-0.1B | 15,000 | 64.7 | 46.5 | (A) |
| | 16,250 | 42.7 | 30.8 | |
| | 20,000 | 21.6 | 71.8 | (A) |
| | " | 20.4 | 21.0 | |
| | 25,000 | 9.3 | 21.0 | |
| Co-35W-3Cr-1Ti-1Zr-0.5C-0.1B -0.1N-0.2Ni | 15,000 | 48.9 | 46.4 | |
| | 20,000 | 15.6 | 39.6 | |
| | " | 16.1 | 33.2 | |
| | 25,000 | 6.0 | 34.8 | |

(A)  Anisotropic deformation assumed, ellipsoidal fracture
     cross-section.

(0)  Heavy oxidation

## TABLE VI- RESULTS OF STRESS-RUPTURE TESTS OF A

## SERIES OF CO-35W-3CR-1TI-1ZR-0.5C-0.1B ALLOY

| Casting Parameters Temperature-°F | | | Initial Stress, Psi | Time To Failure, Hours | Reduction in Area,% | |
|---|---|---|---|---|---|---|
| Superheat (Optical) | Pouring (Optical) | Mold (Actual) | | | | |
| 400 | 300 | 1600 | 15,000 | 154.2 | 22.0 | (0) |
| | | | 20,000 | 33.9 | 51.8 | (A) |
| | | | " | 29.2 | 47.2 | |
| | | | 25,000 | 12.2 | 40.1 | |
| | | | 20,000 | 82.2 | 28.5 | Tested 1800°F |
| | | | 25,000 | 28.6 | 21.8 | " |
| | | | " | 27.3 | 24.5 | " |
| 400 | 200 | 1600 | 15,000 | 131.9 | 51.8 | (0) |
| | | | 17,500 | 50.2 | 47.0 | |
| | | | 20,000 | 24.6 | 60.4 | |
| | | | 22,500 | 16.2 | 52.5 | |
| | | | 25,000 | 9.5 | 39.8 | |
| 300 | 300 | 1600 | 15,000 | 144.3 | 38.0 | (0) |
| | | | 17,500 | 56.6 | 32.1 | |
| | | | 20,000 | 33.1 | 45.8 | |
| | | | 22,500 | 20.4 | 42.5 | |
| | | | 25,000 | 11.8 | 45.0 | |
| 400 | 300 | 1300 | 15,000 | 150.7 | 26.8 | (0) |
| | | | 17,500 | 78.5 | 30.6 | (0) |
| | | | 20,000 | 27.8 | 40.3 | |
| | | | 22,500 | 16.3 | 26.1 | |
| | | | 25,000 | 12.7 | 45.0 | |

(A)  Anisotropic deformation, assumed ellipsoidal fracture cross-section
(0)  Heavy oxidization.

## Table VII
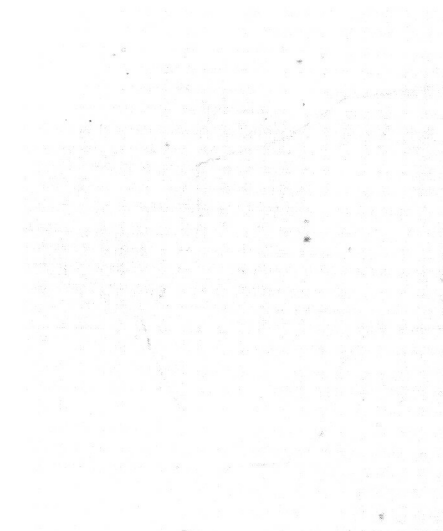
### Mean Free Path and Placro-Grain Size for several Co-35W Base Alloys

| Alloy | Spacing microns | Grain Size (per 1/4" Dia.) | Time to Fracture At 15,000 Psi & 1850°F ( ～Hours ) |
|---|---|---|---|
| Co-35W-0.1B+0.8Ti,0.8Zr,0.2C | 32 | 2-4 | 34.9 |
| Co-35W-0.1B+1Ti, 1Zr,0.5C | 19 | 3-5 | 110.7 |
| Co-35W-0.1B+3Cr, 0.8Ti,0.8Zr,0.5C | 22.5 | 9-12 | 63.5 |
| Co-35W-0.1B+3Cr,1Ti,1Zr,0.5C | 17 | 7-10 | 154.2 |
| | 16.7 | 12-15 | 131.9 |
| | 16.9 | 9-12 | 144.3 |
| | 16.1 | 18-22 | 150.7 |
| Co-35W-0.B+3Cr,2Ti,2Zr,1.0C | 19.4 | 2-4 | 224.9 |
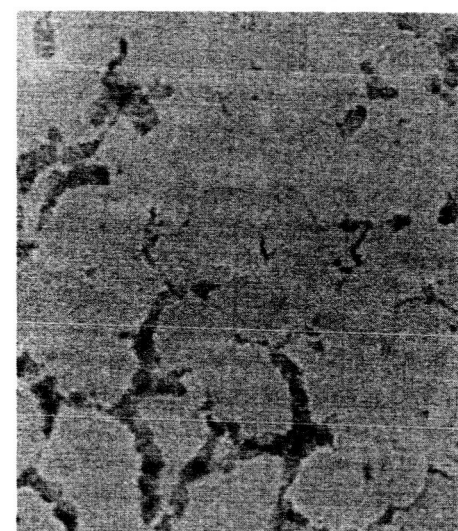
FIG. I: TEST BAR CASTING AND CERAMIC
SHELL MOLD .
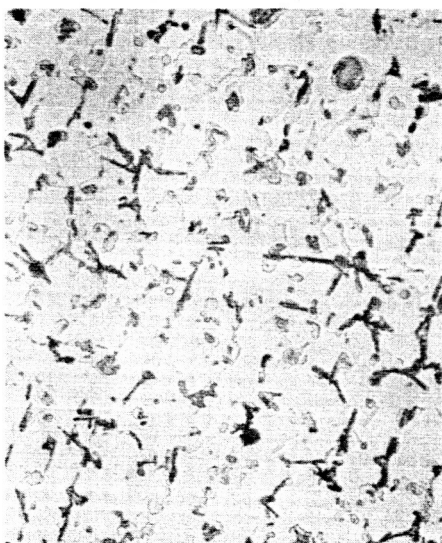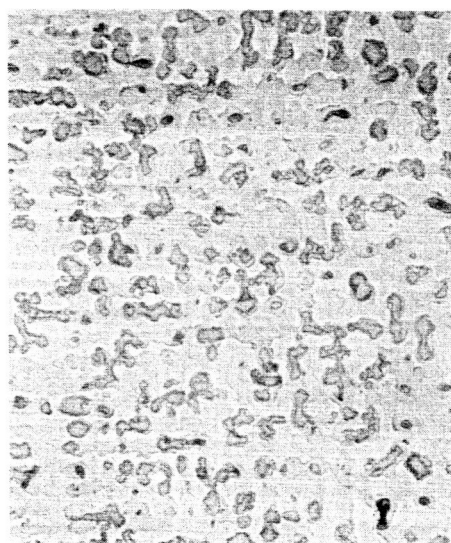
100X

a) Ni-35W, unmodified

100X

b) Ni-40W, unmodified

100X

c) Ni-35W, modified

100X

d) Ni-40W, modified

Figure 2. Ni-W Alloys, from gage section of untested,
cast stress-rupture specimen.

100X

a) Ni-45W, unmodified
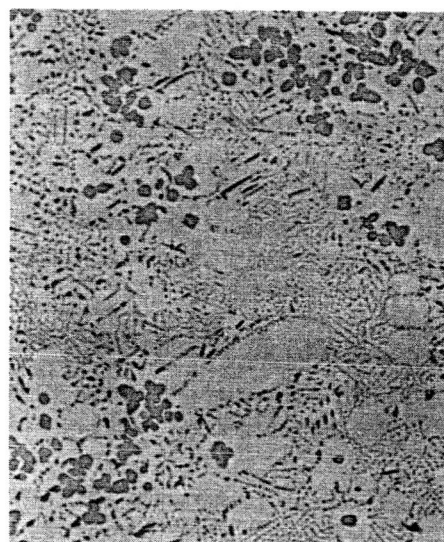


100X

b) Ni-50W, unmodified
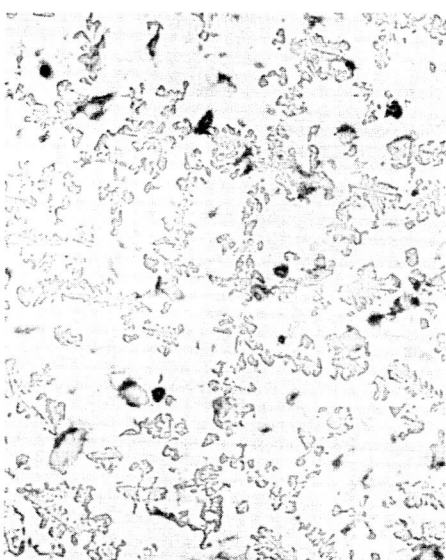


100X

c) Ni-45W, modified
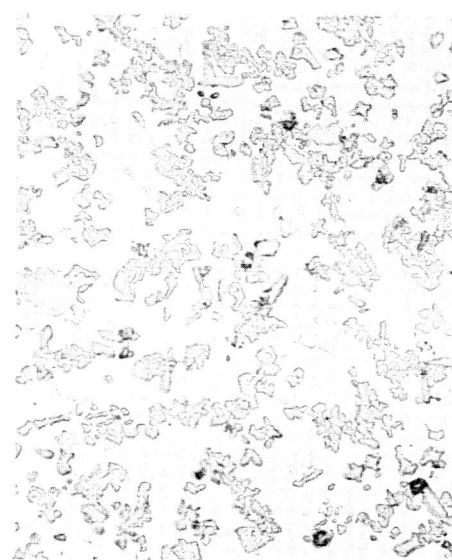


100X

d) Ni-50W, modified

Figure 3.  Ni-W Alloys, from gage section of untested, cast
stress-rupture specimen.
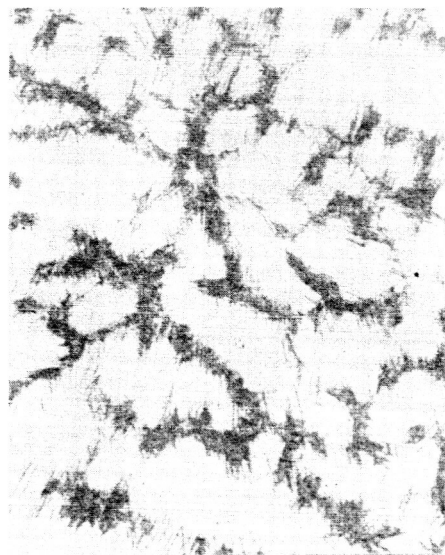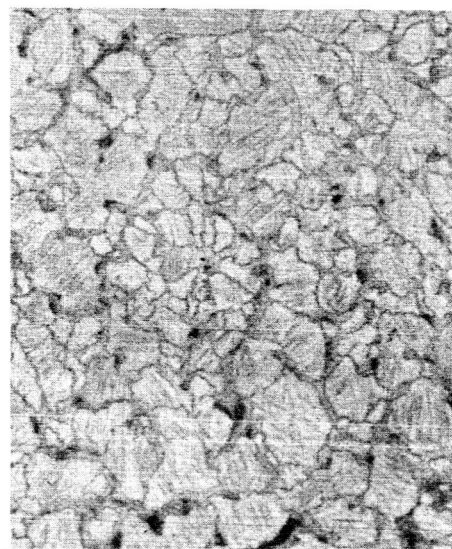
a) Co-35W, unmodified     b) Co-40W, unmodified
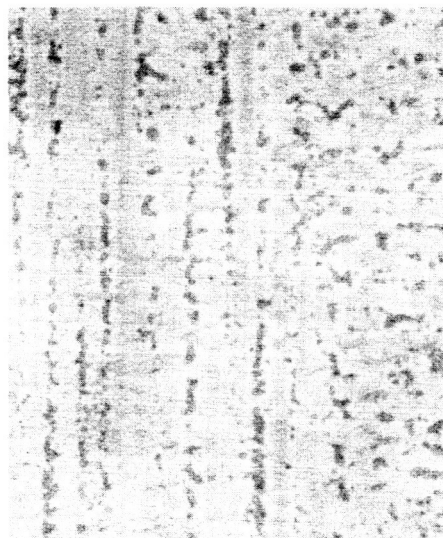
c) Co-35W, modified     d) Co-40W, modified

Figure 4.  Co-W Alloys, from gage section of untested, cast stress-rupture specimen.
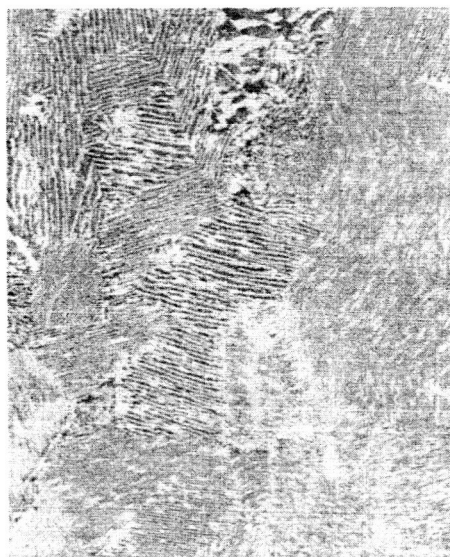
100X

a)  Co-45W,  unmodified



100X

b)  Co-50W, unmodified



100X

c)  Co-45W, modified



100X

d)  Co-50W, modified

Figure 5.  Co-W Alloys, from gage section of untested,
           cast stress-rupture specimen.

FIG. 6 : STRESS – RUPTURE TESTING OF SEVERAL Ni - W AND Co - W ALLOYS
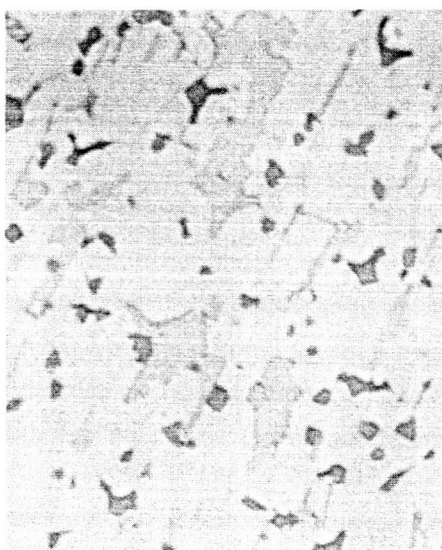(TESTED AT 1800°F IN AIR).
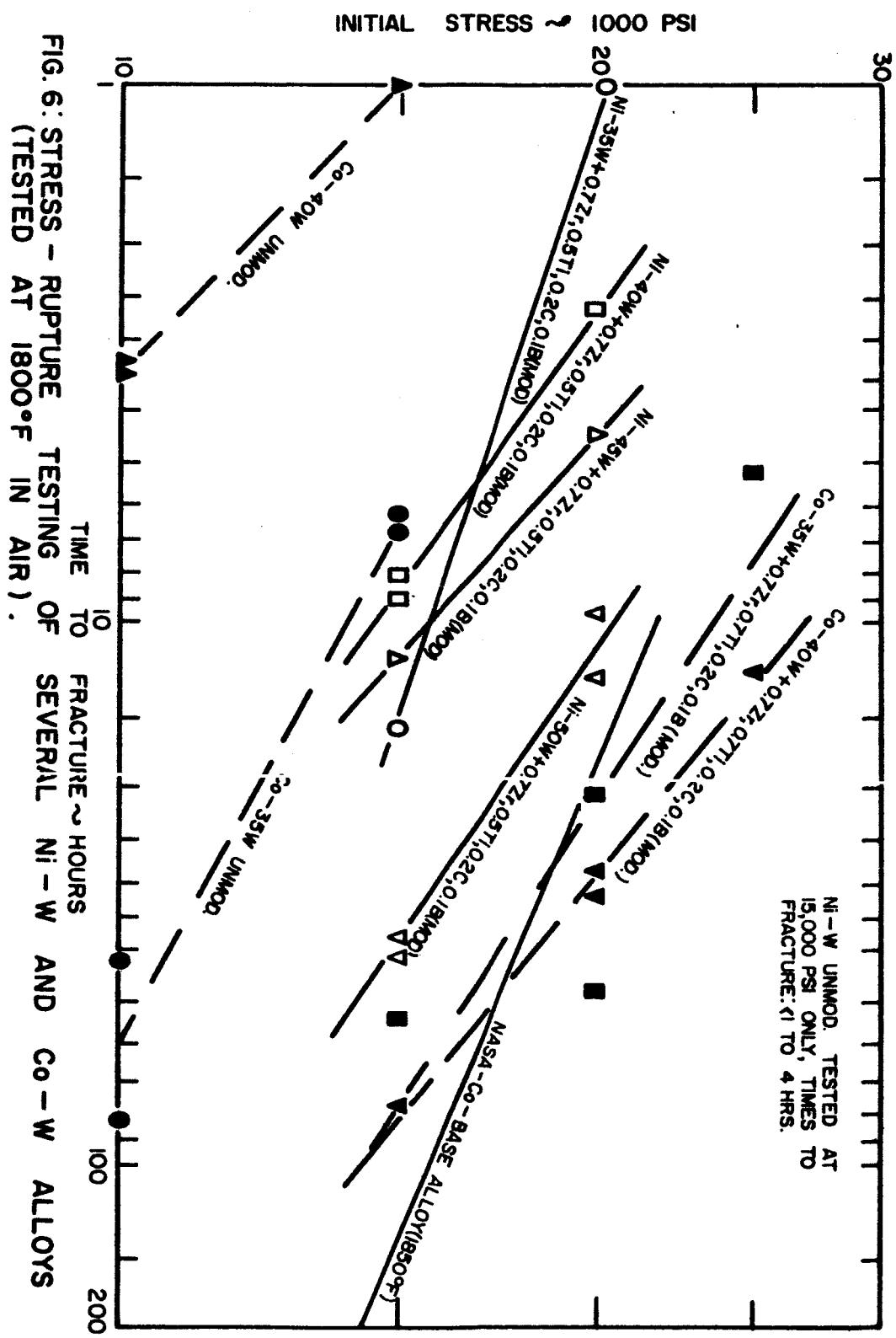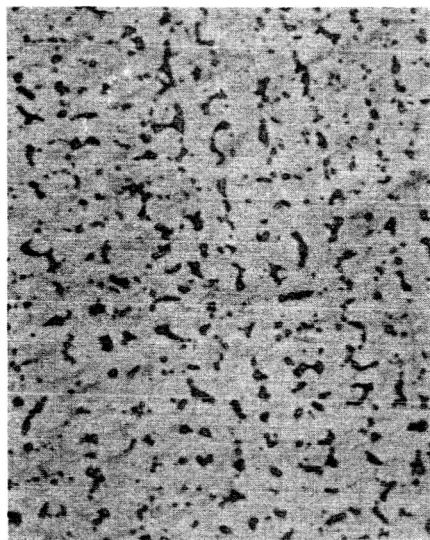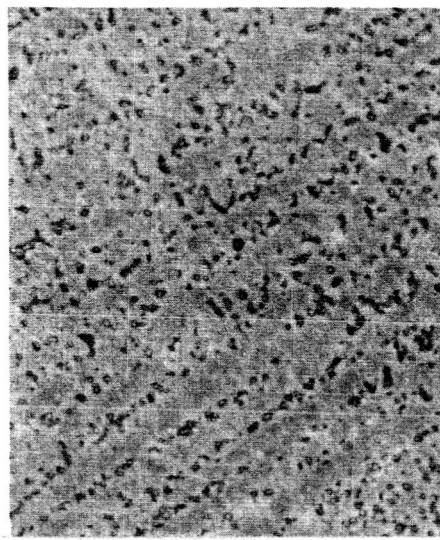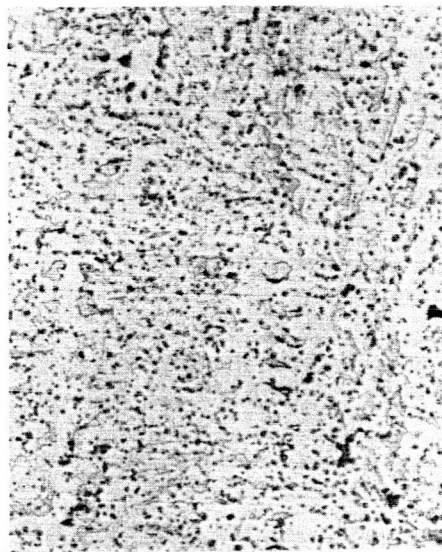
a) As-cast    100X

b) After-testing    100X

c) As-cast    750X

d) After-testing    750X

Figure 7. Co-35W-0.75Ti-0.75Zr-0.2C-0.1B, from gage section of stress rupture specimens.
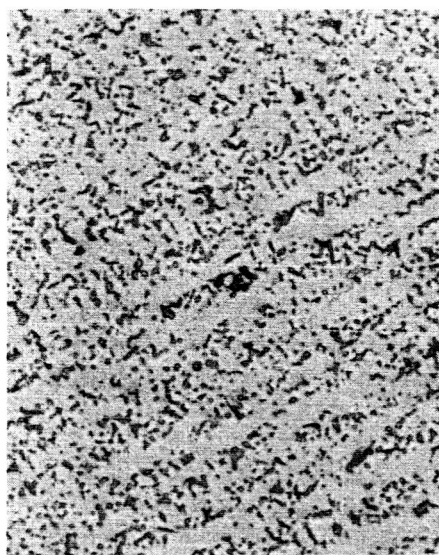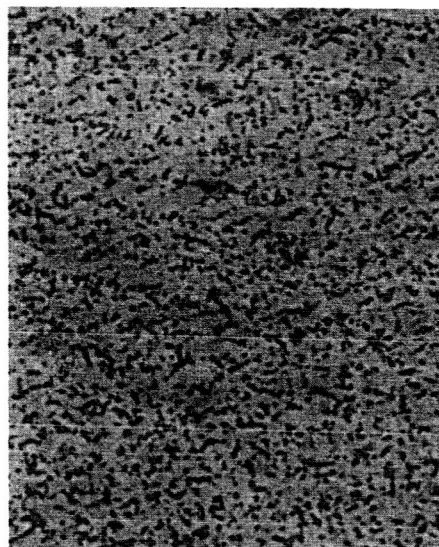
a) As-cast          100X      b) After-testing      100X
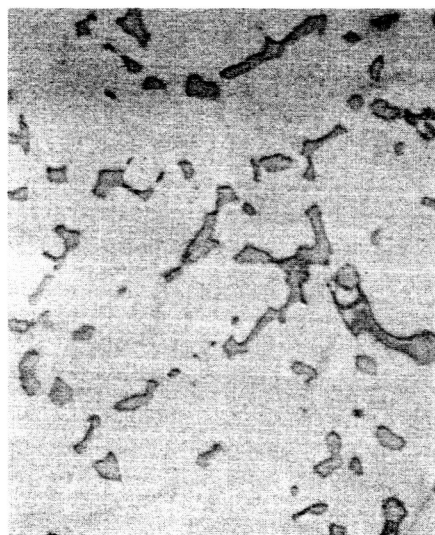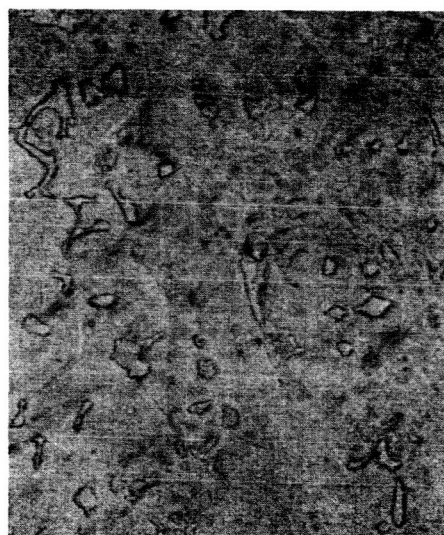
c) As-cast          750X      d) After-testing      750X

Figure 8. Co-35W-1Ti-1Zr-0.5C-0.1B, from gage section of stress rupture specimens.
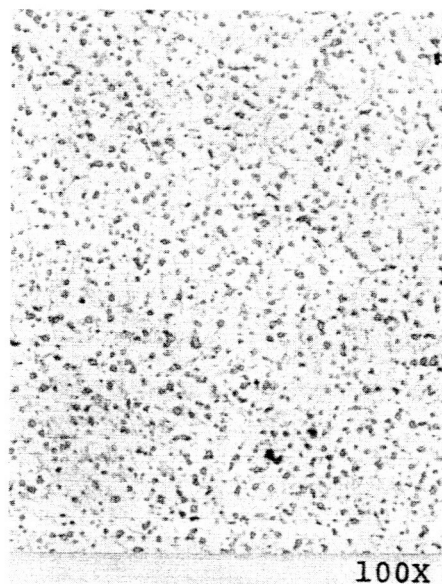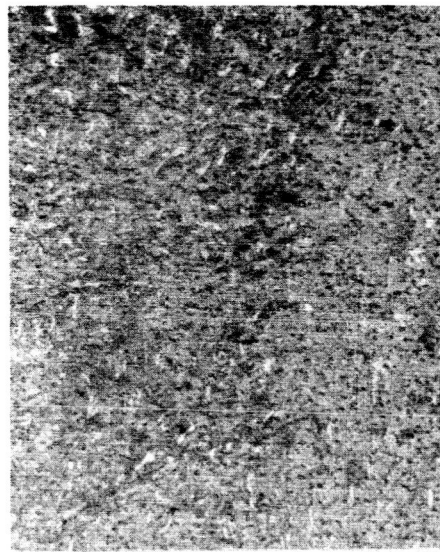
a) As-cast 100X
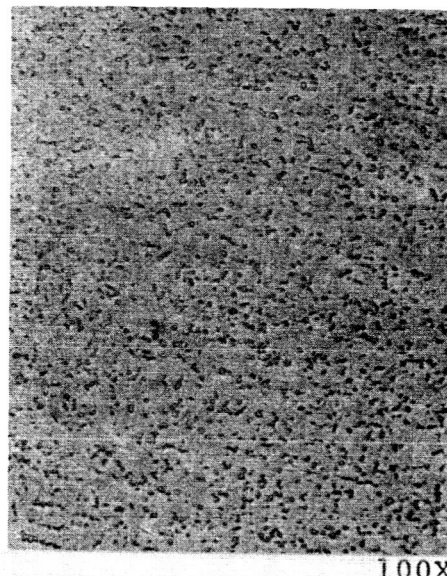
b) After-testing 100X
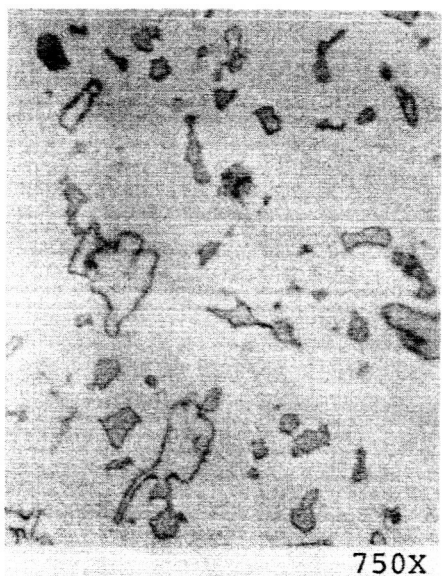
c) As-cast 750X

d) After-testing 750X

Figure 9. Co-35W-3Cr-0.8Ti-0.8Zr-0.5C-0.1B, from gage section of stress rupture specimens.
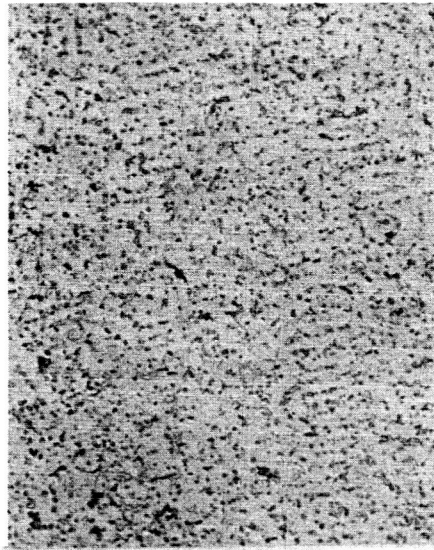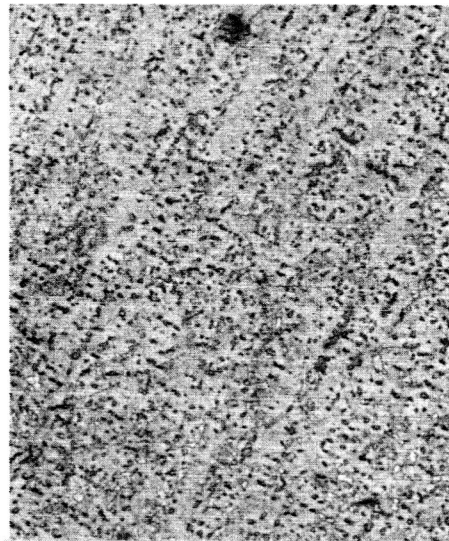
a) As-cast 100X  b) After-testing 100X
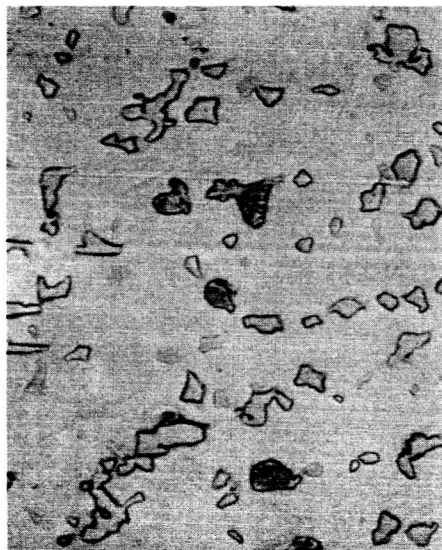
c) As-cast 750X  d) After-testing 750X

Figure 10.  Co-35W-3Cr-1Ti-1Zr-0.5C-0.1B, from gage
section of stress rupture specimens.
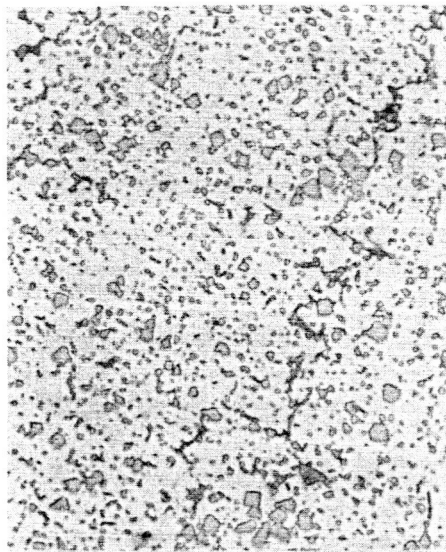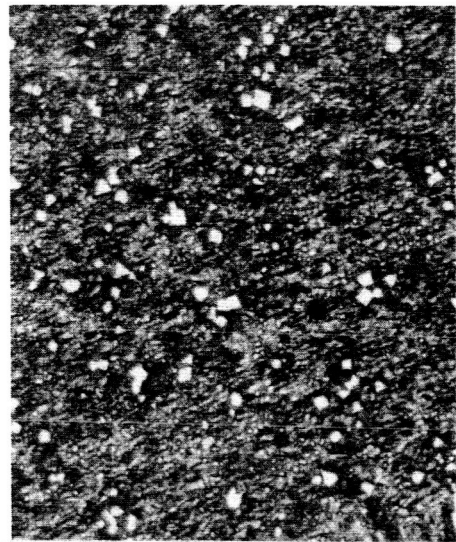
a) As-cast      100X

b) After-testing      100X
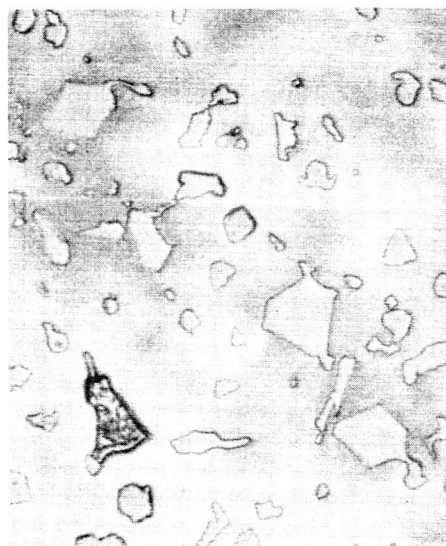
c) As-cast      750X

d) After-testing      750X

Figure 11. Co-35W-3Cr-2Ti-2Zr-1C-0.1B, from gage section of stress rupture specimens.
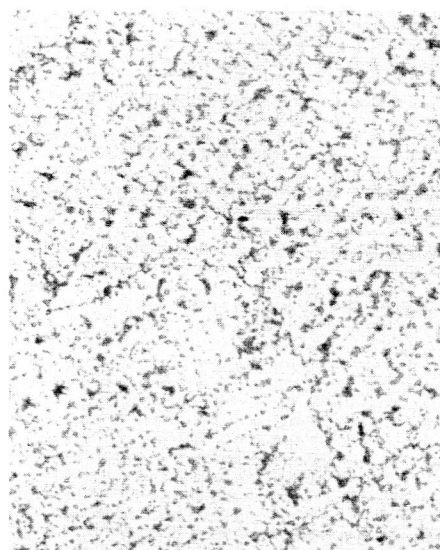
100X

a)  As-cast



750X

b) As-cast

Figure 12.   Co-35W-3Cr-1Ti-1Zr-0.5C alloy, from the gage
section of untested stress rupture specimens.
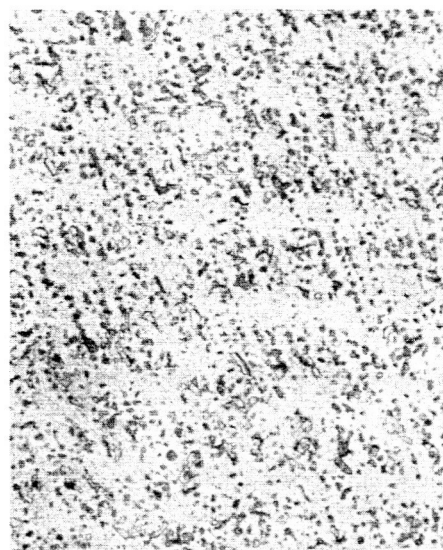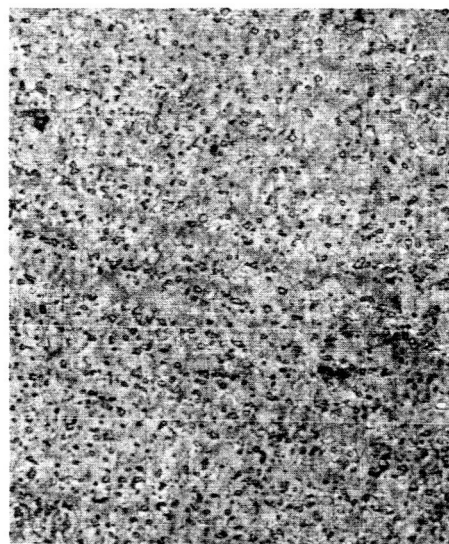
a) As-cast 100X

b) After-testing 100X

c) As-cast 750X

d) After-testing 750X

Figure 13. Co-30W-2.6Mo-1Ti-1Zr-0.5C-0.1B, from gage
sections of stress rupture specimens.
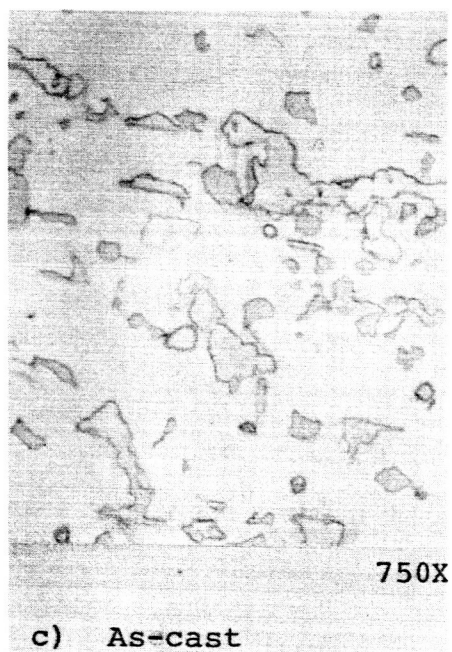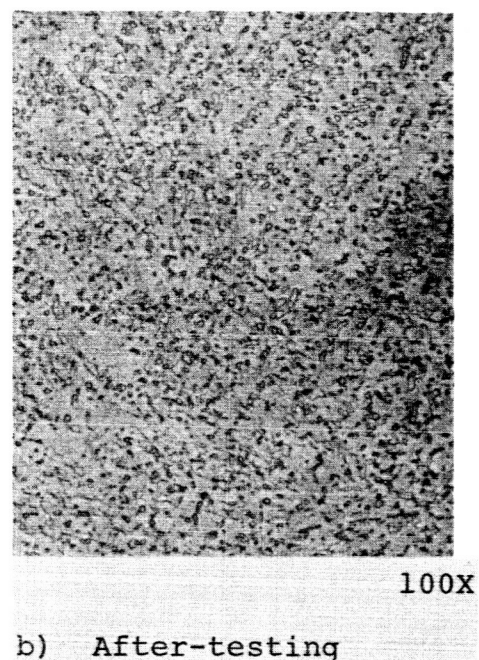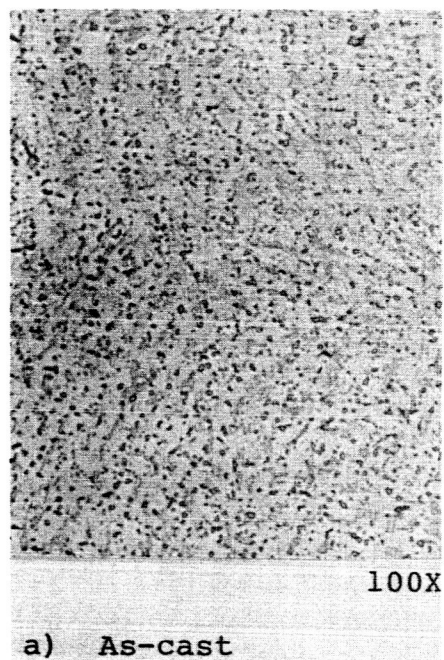
Figure 14. Co-35W-3Cr-1V-1Ti-1Zr-0.5C-0.1B, from gage section of stress rupture specimens.
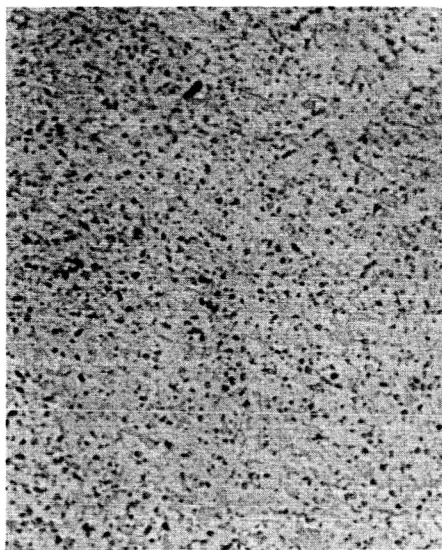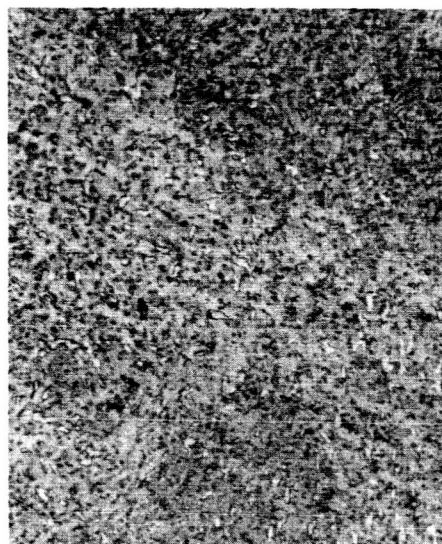
100X

a)  As-cast

100X

b)  After-testing

750X

c)  As-cast

750X

d)  After-testing

Figure 15.   Co-35W-3Cr-2Ta-1Nb-0.5Ti-1Zr-0.5C-0.1B, from
gage section of stress rupture specimens.

100X

a) As-cast

100X
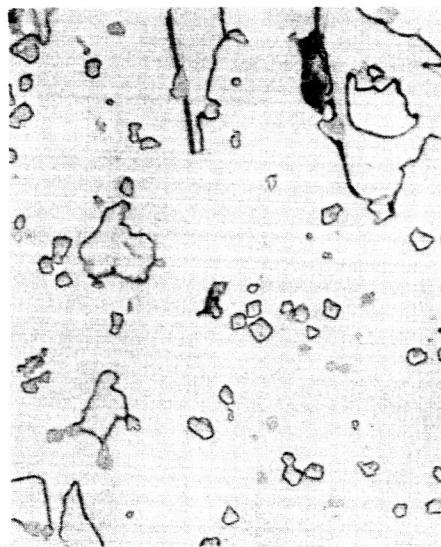
b) After-testing

750X

c) As-cast

750X

d) After-testing

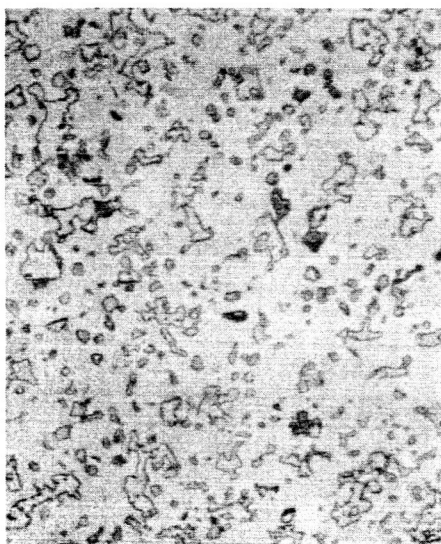Figure 16. Co-35W-3Cr-1Ti-1Zr-0.5C-0.1B-0.1N, from gage section of stress rupture specimens.
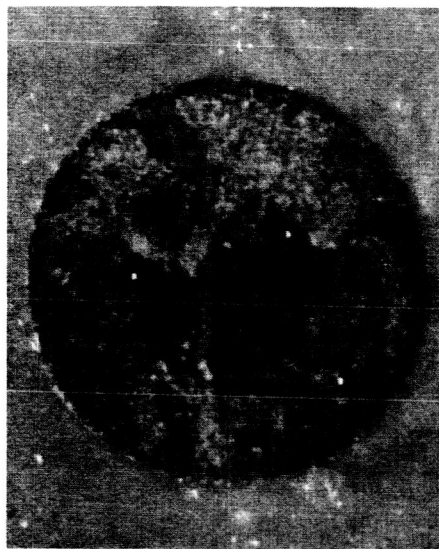
8X

Casting A: 400°F-Superheat
300°F-Pouring; 1600°F-Mold

8X

Casting C:300°F-Superheat
300°F-Pouring; 1600°F-Mold
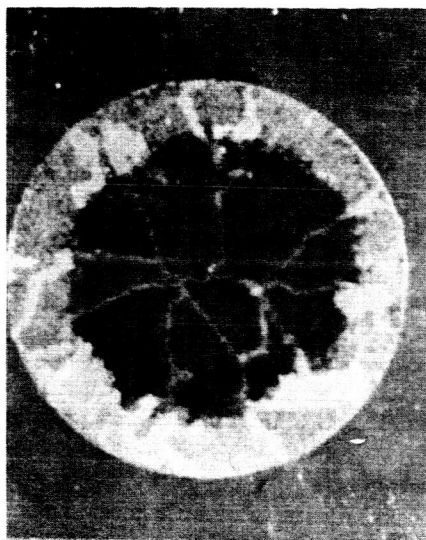
8X

Casting B:    400°F-Superheat
200°F-Pouring; 1600°F-Mold

8X

Casting D: 400°F-Superheat
300°F-Pouring; 1300°F-Mold

Figure 17.    Co-35W-3Cr-1Ti-1Zr-0.5C-0.1B alloy cast under
different conditions, from the gage section of untested
stress rupture specimens.
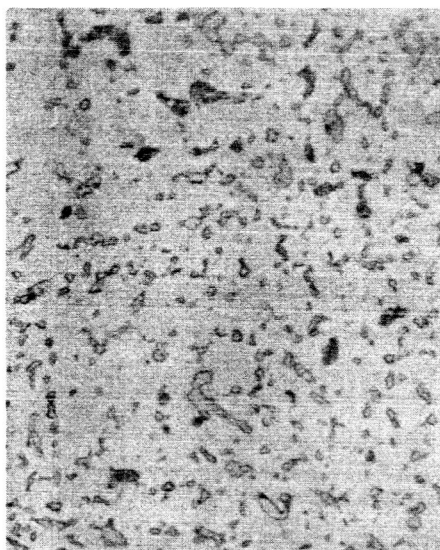
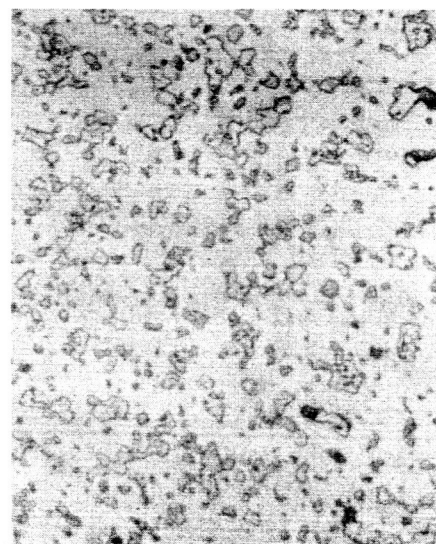250X
Casting A: 400°F-Superheat
300°F-Pouring; 1600°F-Mold
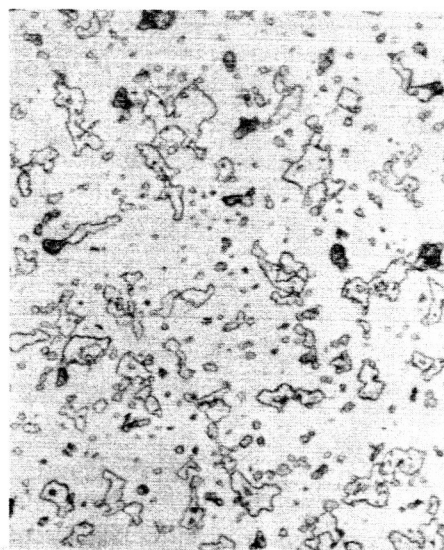
250X
Casting C: 300°F-Superheat
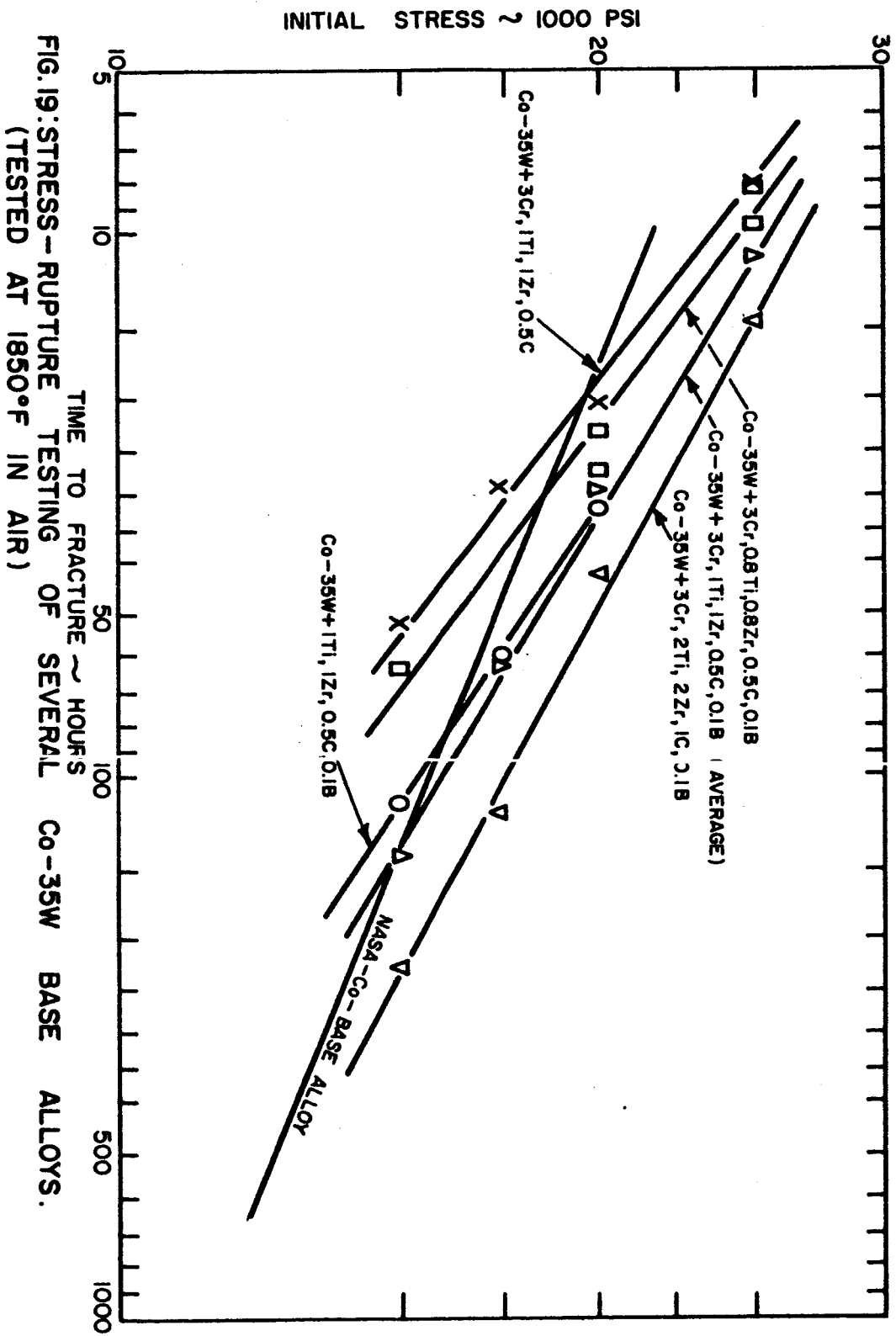300°F-Pouring; 1600°F-Mold

250X
Casting B: 400°F-Superheat
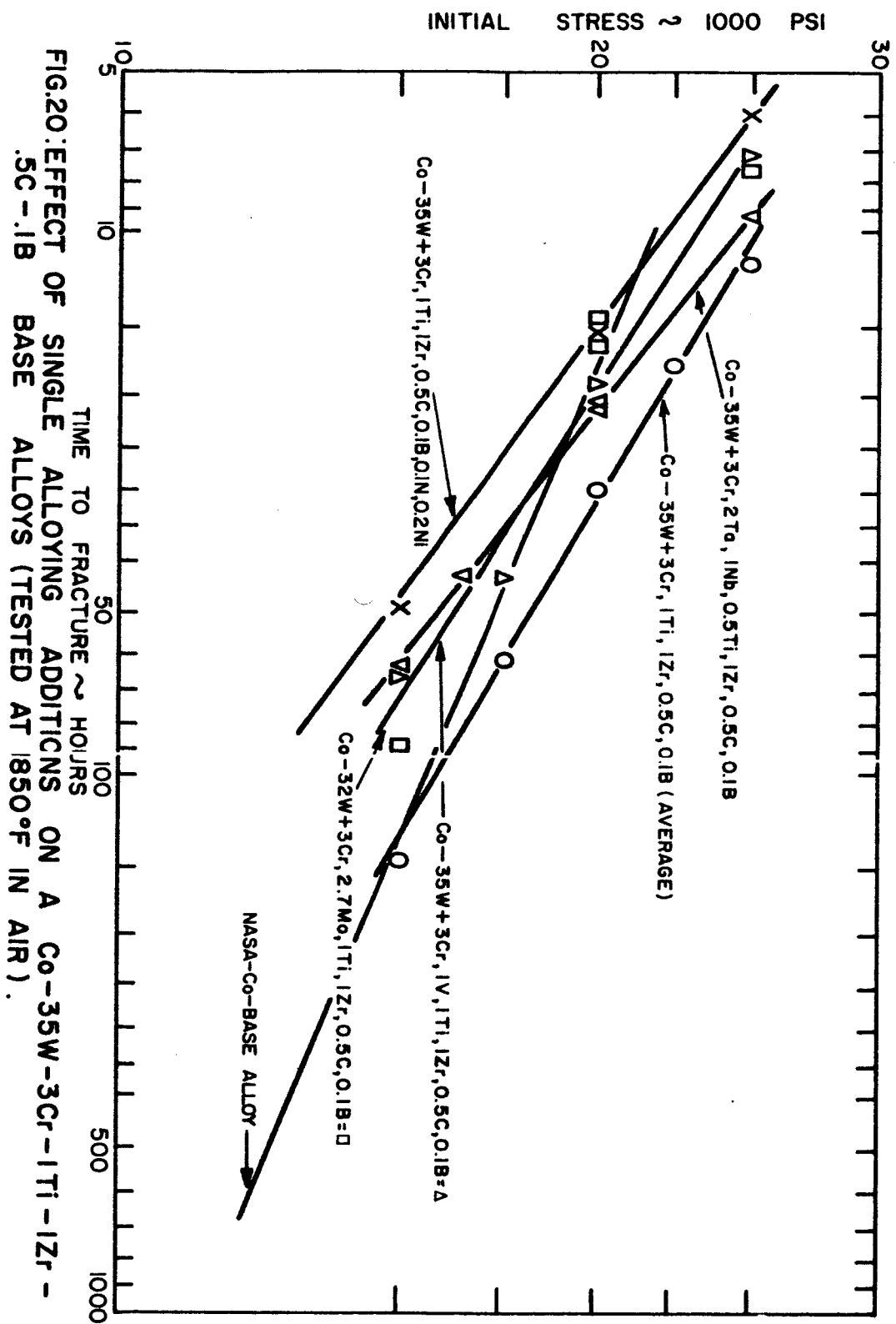200°F-Pouring; 1600°F-Mold

250X
Casting D: 400°F-Superheat
300°F-Pouring; 1300°F-Mold

Figure 18.    Co-35W-3Cr-1Ti-1Zr-0.5C-0.1B alloy cast under
different conditions, from the gage section of untested
stress rupture specimens.

FIG.19: STRESS - RUPTURE TESTING OF SEVERAL Co-35W BASE ALLOYS.
(TESTED AT 1850°F IN AIR )

FIG.20: EFFECT OF SINGLE ALLOYING ADDITIONS ON A Co-35W-3Cr-1Ti-1Zr-.5C-.1B BASE ALLOYS (TESTED AT 1850°F IN AIR).

A        B            C          D        E$_{1X}$

**Figure 21:** Representative Stress Rupture Specimens
After Testing at 20,000 Psi and 1850°F
in Air Showing Different Deformation and
Oxidation Characteristics

A   Co-35W-3Cr-1Ti-1Zr-0.5C-0.1B

**B**   Co-30W-2.6Mo-3Cr-1Ti-1Zr-0.5C-0.1B

C   Co-35W-3Cr-1V-1Ti-1Zr-0.5C-0.1B

D   Co-35W-3Cr-2Ta-1Nb-0.5Ti-1Zr-0.5C-0.1B

E   C0-35W-3Cr-1Ti-1Zr-0.5C-0.1N-0.1B

FIG. 22: EFFECT OF VARIATIONS IN CASTING CONDITIONS ON A Co-35W-3Cr-1Ti-1Zr-0.5C-0.1B ALLOY.
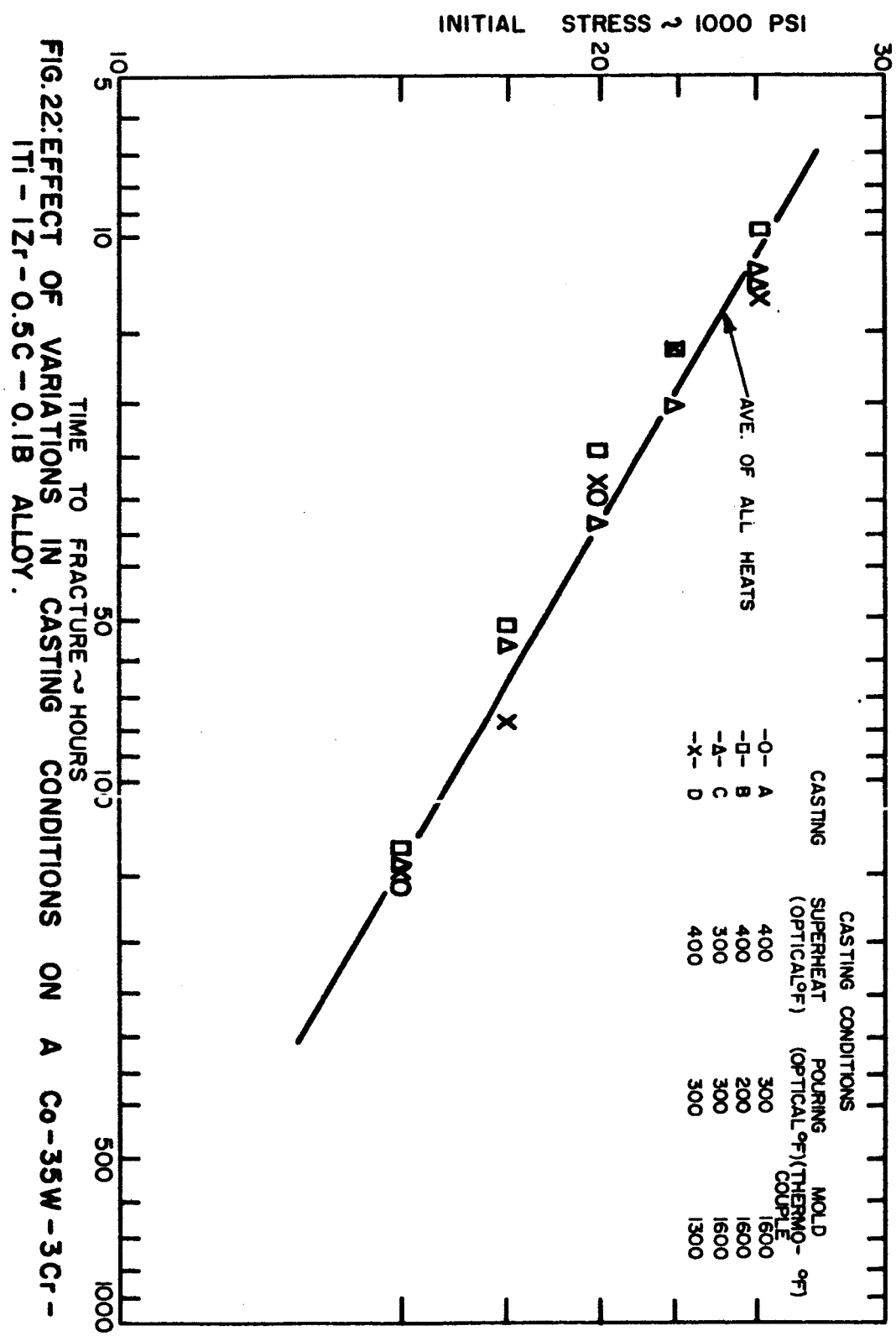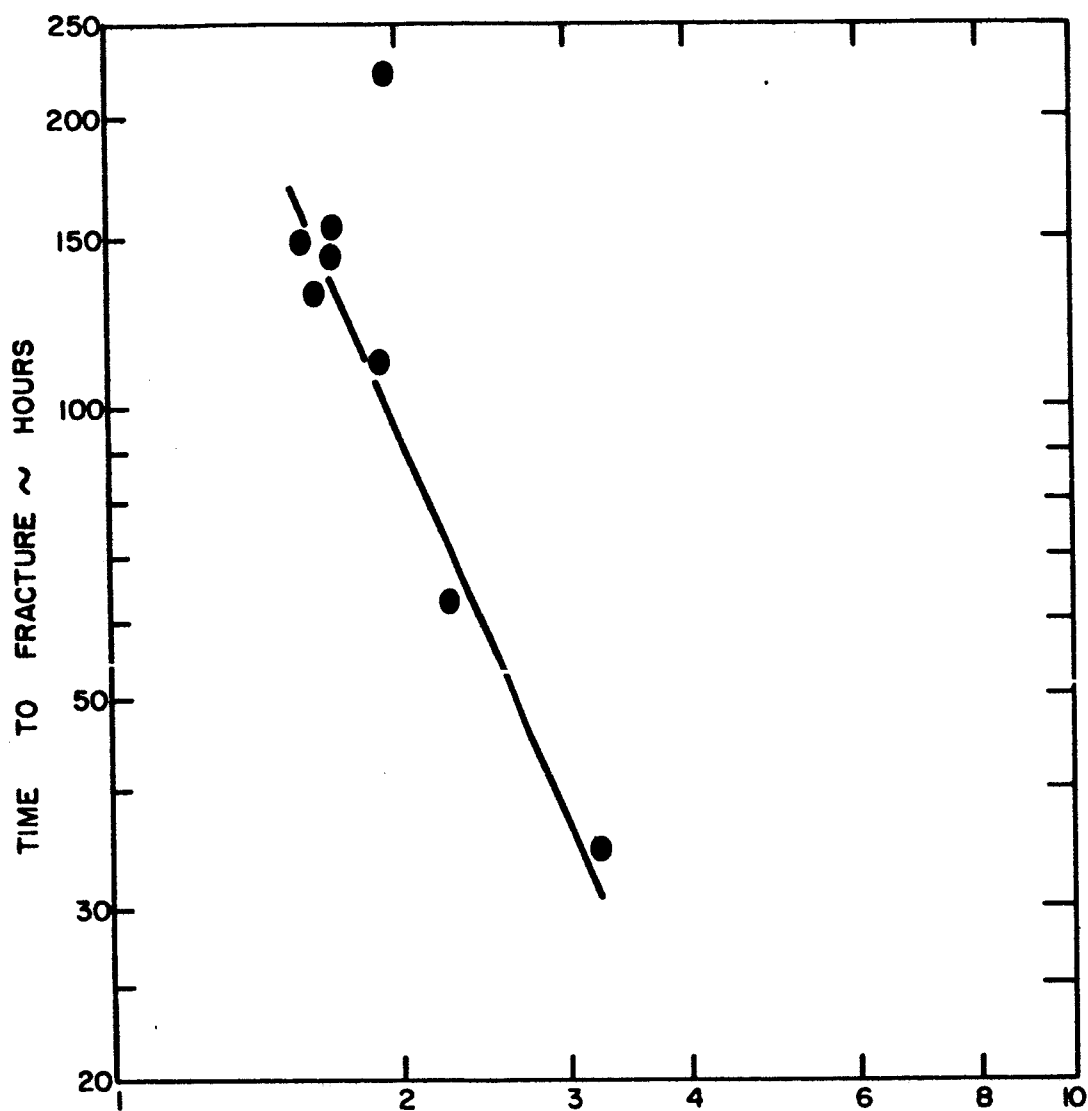
FIG.23: MEAN FREE PATH BETWEEN MICROCONSTITUENTS
OF SEVERAL Co-35W BASE ALLOYS.
(TESTED IN AIR AT 1850°F AND 15,000 PSI
INITIAL STRESS)